Highly Efficient Red Emitting OLEDs Prepared from Nona-Coordinated Europium(III) Complexes

Rashid Ilmi,*[a] Xiaoyang Xia,[b] José D. L. Dutra,[c] Gabriel Silva Santos,[c] Liang Zhou,*[b] Wai-Yeung Wong,*[d] Paul R. Raithby*[e], and Muhammad S. Khan*[a]

[a]Department of Chemistry, Sultan Qaboos University, P. O. Box 36, Al Khod 123, Oman

[b]State Key Laboratory of Rare Earth Resource Utilization, Changchun Institute of Applied Chemistry, Chinese Academy of Sciences, Renmin Street 5625, Changchun 130022, People's Republic of China.

[c]Pople Computational Chemistry Laboratory, Department of Chemistry, UFS, 49100-000 São Cristóvão, Sergipe, Brazil.

[d]Department of Applied Biology and Chemical Technology and Research Institute for Smart Energy, The Hong Kong Polytechnic University, Hung Hom, Kowloon, Hong Kong, People's Republic of China.

[e]Department of Chemistry, University of Bath, Claverton Down, Bath, BA2 7AY, UK

Corresponding authors information: Name: E-mail;ORCID ID

Rashid Ilmi (RI) : rashidilmi@gmail.com; 0000-0002-5165-5977

Liang Zhou (LZ) : zhoul@ciac.ac.cn; 0000-0002-2751-5974

Wai-Yeung Wong (WYW) : wai-yeung.wong@polyu.edu.hk; 0000-0002-9949-752

Paul R. Raithby : p.r.raithby@bath.ac.uk; 0000-0002-2944-0662

Muhammad S. Khan (MSK) : msk@squ.edu.om; 0000-0001-5606-6832

Abstract: We have designed and synthesized three nona-coordinated organoeuropium complexes (OEuCs) with the general formula [Eu(btfa)$_3$(FurTerPy)] (**Eu1**), [Eu(btfa)$_3$(ThioTerPy)] (**Eu2**) and [Eu(btfa)$_3$(NapTerPy)] (**Eu3**) by employing a primary 4,4,4-trifluoro-1-phenyl-1,3-butanedione (btfa) antenna ligand and three functionalized 2,2′:6′,2″-terpyridine (TerPy) ligands bearing different electron-donating groups at the 4' position, namely, FurTerPy = 4'-(furan-2-yl)-2,2':6',2''-terpyridine; ThioTerPy = 4'-(thiophen-2-yl)-2,2':6',2''-terpyridine; and NapTerPy = 4'-(naphthalen-1-yl)-2,2':6',2''-terpyridine. Detailed photophysical properties of **Eu1**, **Eu2** and **Eu3** were analysed using both experimental and computational methods. By analysing the experimental and time-dependent density functional theory (TD-DFT) data in conjunction with the Lanthanide Luminescence Software Package (LUMPAC), we further elucidated the energy transfer (ET) processes in the OEuCs. Finally, the complexes were tested as emitting layer (EML) in a multi-layered device to fabricate red organic light emitting diodes (R-OLED). Through the optimization and device engineering, we have achieved a remarkable electroluminescence (EL) performance of maximum current efficiency (η_c) = 12.32 cd/A; maximum power efficiency (η_p) = 11.73 lm/W and maximum external quantum efficiency ($EQE_{max.}$) = 10.20%, respectively, for the **Eu3**-based double-EML OLED. To the best of our knowledge, this is the highest reported overall EL performance among the OEuCs until now.

Keywords: 4,4,4-trifluoro-1-phenyl-1,3-butanedione**;** Terpyridine**;** Europium(III); Energy transfer mechanism; Red electroluminescence; Carrier trapping; Förster energy transfer

Introduction

The establishment of the photoluminescence (PL) properties of organo-lanthanide complexes have strengthened their position among the many available functional materials and makes them suitable for potential technological applications, particularly organoeuropium complexes (OEuCs) in OLEDs,[1, 2, 3] as sensors,[4] as sensitizers to improve the OLED performance of the state-of-the-art red-emitting iridium(III) complexes.[5] and as luminescent thermometers.[6, 7] Among the large number of monochromatic red emitting OEuCs, easily obtainable tris(β-diketonato)Eu(III) complexes incorporating polydentate ancillary ligand(s) [*N^N/O^O/N^N^N/O^O^O*][8, 9] could provide a cheap and environmental-friendly alternative to the sought after red-emitting phosphorescent complexes[10, 11, 12] and thermally activated delayed fluorescence (TADF)[13, 14] materials that dominate OLED field. This is due to their innate photophysical properties, specifically their highly monochromatic red emission with full width at half maxima (FWHM) < 15 nm ensuing excellent colour purity and high photoluminescence quantum yields (PLQYs).[15, 16] Another important prerequisite for developing efficient OLEDs is the good electron-transport properties of the compounds/complexes in question.[16] Apart from synthesis, purification of OEuCs is relatively very easy compared to the aforementioned materials which need specific synthetic modifications to reach targeted wavelength maxima (red emission = 605 – 650 nm) coupled with complicated purification procedures.[17, 18] The former materials have very short excited state lifetimes of a few microseconds to sub-microsecond[18] compared to that of homoleptic and heteroleptic OEuCs, which exhibit higher excited state lifetimes in the 1 – 3 millisecond (ms)[19, 20] and 100 – 900 microsecond (μs) range.[21, 22]

Interestingly, a literature survey further revealed that the most dominant OEuCs among the many heteroleptic complexes are octacoordinated neutral tris(β-diketonato) complexes incorporating different ancillary ligands (*N^N*/*O^O* etc.)[23, 24] and have been successfully employed as EML to fabricate R-OLEDs.[8, 9] It is noteworthy that the EL in the OEuCs was first reported by Kido and co-workers[25, 26] more than three decades ago; however, the EQE of R-OLEDs comprising OEuCs is still not very satisfactory. Despite this long research journey, to date, only an EQE_{max} of 7.5% was achieved by a [$Eu(dbm)_3$BPhen]-based[27] device (**Chart 1**, dbm is the anion of dibenzoylmethane and BPhen = Bathophenathroline). To improve the EL performance of OEuCs, our research group has recently embarked on the design, development and device engineering of efficient OEuCs to improve overall EL performance. By employing a large bite angle of bis[2-(diphenylphosphino)phenyl] ether oxide (DPEPO) [O^O] as the ancillary ligand and 4,4,4-trifluoro-1-phenyl-1,3-butanedione (Hbtfa) and 4,4,4-trifluoro-1-(2-naphthyl)-1,3-butanedione (Hnta) as the primary antenna ligands, two octacoordinated OEuCs, [$Eu(btfa)_3$(DPEPO)] and [$Eu(nta)_3$(DPEPO)] (**Chart 1a**) were synthesized and successfully employed as EML to fabricate R-OLEDs.[15] Through the device engineering i.e., the combination of proper host materials, the double-EML device of [$Eu(nta)_3$(DPEPO)] at the optimum doping concentration (4 wt%) exhibited pure red EL with

a EQE_{max} of 6.3%. To further improve the EL performance, we have recently synthesized two highly efficient octacoordinated red-emitting OEuCs (**Chart 1a**) by exploiting the rigid neutral hole or exciton-blocking BPhen (N^N) (triplet state ($^3\pi\pi^*$) = 21000 cm^{-1}; electron mobility = 5 × 10^{-4} cm^2 V^{-1} s^{-1})[28, 29] as the ancillary ligand in conjunction with Hbtfa and 2-thenoyltrifluoroacetone (Htta) as the primary antenna ligands.[16] The double-EML R-OLEDs of [Eu(btfa)$_3$BPhen][16] and [Eu(tta)$_3$BPhen][16] exhibited impressive $EQE_{max.}$ = 5.91% and 6.24%, respectively, at very low doping concentration (2 wt%). It was further observed that the brightness (B) of the device in a given complex-based device is independent of the PLQY of the complex:host film and depends on the excited state lifetime (τ_{obs}) of the complex:host film.

As mentioned above the octacoordinated [Eu(β-diket.)$_3$(*N^N*/*O^O* etc)] complexes are the dominant class of OEuCs. Moreover, it is worth remembering that the bulk of the work is based on either 'tta' or 'dbm' as the primary antenna ligand and thus the potential of other β-diketone based OEuCs remains uncharted for this purpose.[30] Keeping this idea in mind and our quest to improve the EL performance of OEuCs, we recently designed and synthesized two novel asymmetric nonacoordinated complexes[31] by employing btfa and nta as primary antenna ligands and a simple 4'-phenyl-2,2':6',2''-terpyridine (Ph-terPy) ligand with the general formula [Eu(btfa)$_3$(Ph-terPy)] and [Eu(nta)$_3$(Ph-terPy)] (**Chart 1a**). The prime advantage of nonacoordinated complexes over octacoordinated complexes is their lower molecular symmetry, which according to Judd-Ofelt (J-O) theory[32, 33] is propitious in reducing τ_{obs} and thus could be beneficial for generating good EL performance.[15] This is because forbidden 4f – 4f electronic transitions become partially allowed and directly related to the orbital mixing between the 4f and 5d orbitals.[34] The double-EML OLEDs of [Eu(nta)$_3$(Ph-terPy)] (3 wt.%), displayed an outstanding EL performance reaching EQE_{max}. of 7.32 %.[31] Insights gained during our exploration and our continuing research dedicated to improve the EL performance of OEuCs, led us in the present studies, to synthesise three functionalized 2,2':6',2''-terpyridine (TerPy) ancillary ligands by installing electron-rich furan, thiophene and naphthalene moieties at the 4' position of TerPy. The ancillary ligands were utilized to develop three new nonacoordinated asymmetric OEuCs in conjunction with the primary antenna 'btfa' ligand having the general formula [Eu(btfa)$_3$(FurTerPy)] (**Eu1**), [Eu(btfa)$_3$(ThioTerPy)] (**Eu2**) and [Eu(btfa)$_3$(NapTerPy)] (**Eu3**) (**Chart 1b**). The complexes were characterized prior to their potential application as EML to fabricate R-OLEDs, the photophysical properties of the complexes were evaluated and are discussed in detail. Moreover, with the help of experimental photophysical properties and theoretical methods using density functional theory (DFT) and TD-DFT in conjunction with the LUMPAC,[35] the energy migration processes involved were elucidated and discussed for the complexes. Finally, the complexes were employed as EML to fabricate OLEDs and their EL performance parameters such as brightness (B), current efficiency (η_c), power efficiency (η_p), EQE and CIE colour coordinates were analysed and discussed.

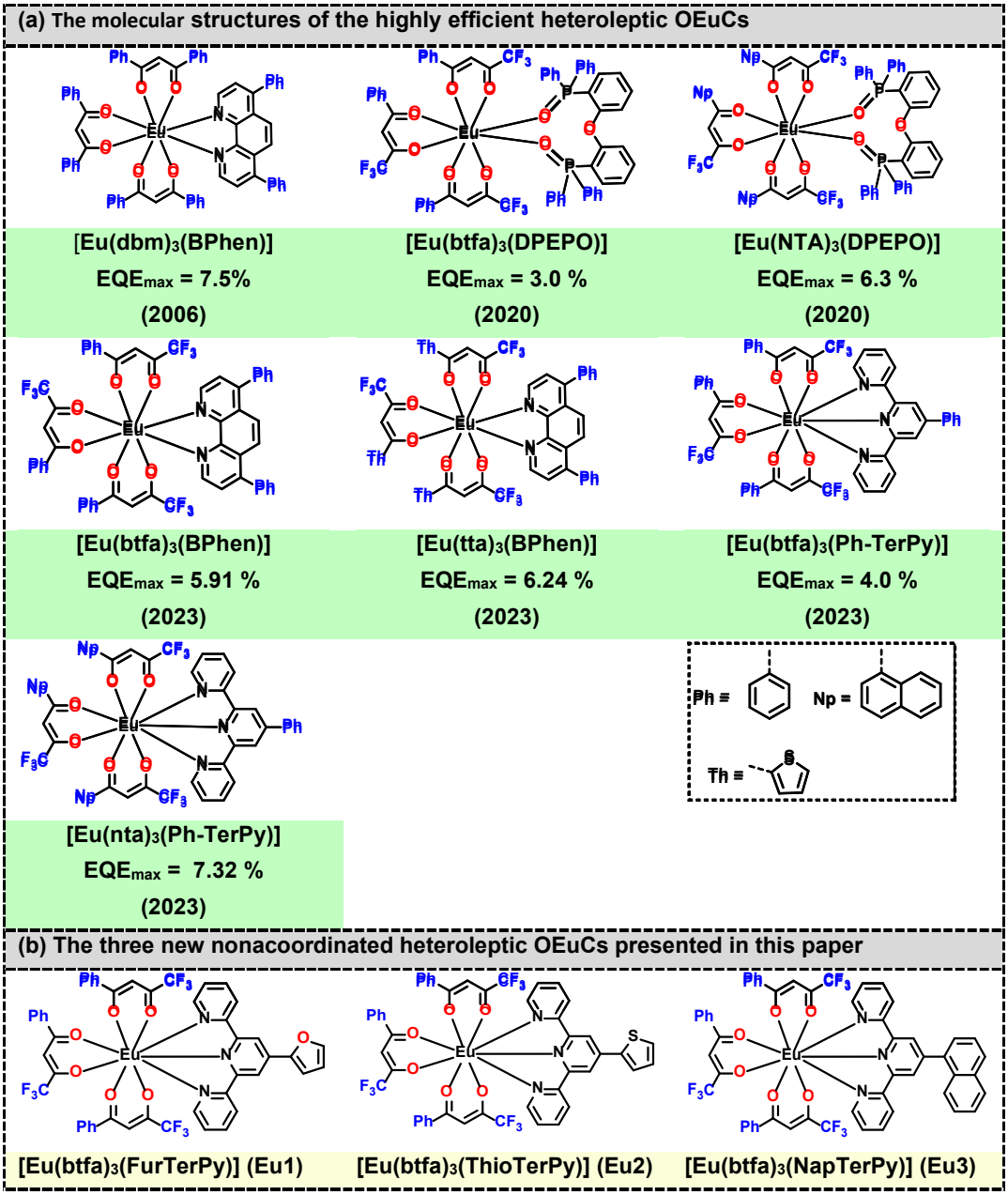

Chart 1: (a) The molecular structures of the highly efficient heteroleptic OEuCs utilized to fabricate R-OLEDs with their EQE_{max}. and (b) The chemical structures of the three new nonacoordinated heteroleptic OEuCs.

Details of the Experimental Methods

Chemical, Reagents and General Instrumentation

All chemicals used in the synthesis and the OLED fabrication were procured from commercial sources and were used without further purification unless otherwise specified. Solvents used in the experiments were dried and distilled prior to use.[36] Elemental analysis was performed on a Euro EA−CHN Elemental Analyser. The Fourier transform infrared (FT-IR) spectra of the solid ligands and OEuCs were obtained using a Cary 630 FT-IR spectrometer in the attenuated total reflectance (ATR) mode. The mass spectra were

obtained using a Bruker autoflex III smartbeam MALDI-TOF/TOF mass spectrometer. Nuclear magnetic resonance (NMR) spectra were recorded on Bruker Biospin Avance III HD (700 MHz) FT-NMR spectrometer in $CDCl_3$ with $SiMe_4$ as the internal reference.

Synthesis of Ancillary Ligands

4'-(Furan-2-yl)-2,2':6',2''-terpyridine (**FurTerPy**): The terpyridine ligands were synthesized by following the synthetic protocol reported previously.[31] A general synthetic approach for 4'-(furan-2-yl)-2,2':6',2''-terpyridine (FurTerPy) is described here as a representative of other TerPy ligands. Briefly, to a stirred solution of furan-2-carbaldehyde (1.8422 g; 17.36 mmol) and 2-acetylpyridine (4.2084 g, 34.74 mmol) in ethanol (EtOH, 50 mL), potassium hydroxide (KOH; 1.95 g; 38.50 mmol) and 25% ammonia solution (15 mL) were added. The reaction mixture was stirred for 24 h at room temperature. The precipitate formed was isolated by vacuum filtration and washed with a copious amount of distilled water, followed by EtOH (50 mL × 3). The compound was purified by silica column chromatography by first eluting with hexane to remove the unreacted furan-2-carbaldehyde and then eluting with dichloromethane (CH_2Cl_2): methanol (MeOH) [95:5]. The obtained light brown solid was recrystallized from (CH_2Cl_2): EtOH (1:1) as light brown needles (55% yield). Analysis calculated for $C_{19}H_{13}N_3O$, C, 76.24; H, 4.38; N, 14.04; observed C, 76.22; H, 4.35; N, 14.02%; other data matches very well with literature values[37] FT-IR: $\nu_{C=N} + \nu_{C=C}$; 1582 cm^{-1} (**Figure S1a, ESI**). ^1H NMR (700 MHz, $CDCl_3$, δ/ppm): 8.69 (m; 2-H, 6,6'); 8.68 (s; 2-H, 3',5'); 8.59 (d, 2-H, 3,3'); 7.83 (td, 2-H, 4,4'); 7.53 (d, 1-H; 7 from furan); 7.31(m, 2-H, 5,5'); 7.09 (d, 1-H; 9 from furan); 6.50 (q, 1-H, 8 from furan) (**Figure S2a, ESI**). ^{13}C NMR (175 MHz, $CDCl_3$, δ/ppm) 155.85, 155.68, 151.83, 148.93, 143.86, 139.68, 137.24,124.02, 121.47, 115.33, 112.21, 109.09 (**Figure S2b, ESI**).

4'-(Thiophen-2-yl)-2,2':6',2''-terpyridine (ThioTerPy): ThioTerPy was synthesized and purified by a similar method and data matches well with literature values.[37] Analysis calculated for $C_{19}H_{13}N_3S$, C, 72.36; H, 4.15; N, 13.32; observed C, 72.35; H, 4.12; N, 13.31%. FT-IR: $\nu_{C=N} + \nu_{C=C}$; 1582 cm^{-1} (Figure S1b, ESI). ^1H NMR (700 MHz, $CDCl_3$, δ/ppm): 8.68 (m; 2-H, 6,6'); 8.64 (s; 2-H, 3',5'); 8.58 (tt, 2-H, 3,3'); 7.88 (td, 2-H, 4,4'); 7.53 (dd, 1-H; 7 from thiophene); 7.30 (m, 2-H, 5,5'); 7.09 (dd, 1-H; from thiophene); 7.11 (q, 1-H, from thiophene) (**Figure S3a, ESI**). ^{13}C NMR (175 MHz, $CDCl_3$, δ/ppm) 155.85, 155.68, 151.83, 148.93, 143.86, 139.68, 137.24,124.02, 121.47, 115.33, 112.21, 109.09 (**Figure S3b, ESI**).

4'-(Naphthalen-1-yl)-2,2':6',2''-terpyridine (NapTerPy): NapTerPy was synthesized and purified by a similar method and data matches well with literature values.[38] Microanalysis calculated for $C_{25}H_{17}N_3$, C, 83.54; H, 4.77; N, 11.69; observed C, 83.52; H, 4.78; N, 11.68; FT-IR: $\nu_{C=N} + \nu_{C=C}$; 1582 cm^{-1} (Figure S1c, ESI). ^1H NMR (700 MHz, $CDCl_3$, δ/ppm): 8.82 (s; 2-H, 3',5'), 8.70 (m; 2-H, 6,6'); 8.65 (d, 2-H, 3,3'); 8.36 (b, 1-H for 9 from napthalene); 7.98 (b, 1-H for 10 from napthalene)) 7.93 (d, 2-H for 4,4'); 7.86 – 7.80 (m, 3-H from naphthalene); 7.50 – 7.45 (m, 2-H from naphthalene); 7.32 (m, 2-H, 5,5') (**Figure S4a, ESI**).

^{13}C NMR (175 MHz, $CDCl_3$, δ/ppm) 156.11, 155.88, 150.23, 149.02, 137.21, 135.64, 128.75, 128.66, 127.33, 126.81, 126.74, 126.55, 125.01, 124.00, 121.59, 119.22 (**Figure S4b, ESI**).

Synthesis of Neutral Ternary Europium(III) Complexes

[Eu(btfa)$_3$(FurTerPy)] (Eu1): Eu1 was synthesized by reacting equimolar quantities of [Eu(btfa)$_3$(H_2O)$_2$][15] (0.300 g; 0.360 mmol) and FurTerPy (0.111 g; 0.360 mmol) in methanol (MeOH; 20 mL). The reaction mixture was stirred overnight at room temperature and left for slow solvent evaporation. The solid formed was washed with cold EtOH (5 × 2 mL) and toluene (5 × 2 mL). Yield 80%. Analysis calculated for $C_{51}H_{33}EuF_9N_3O_6$, C, 55.35; H, 3.01; N, 3.80; observed C, 55.40; H, 3.08; N, 3.76%. FTIR (solid; cm^{-1}): $\nu_{(ar\ C\text{-}H\ st)}$ 3074 cm^{-1}; $\nu_{(C=O\ st)}$ 1,612 cm^{-1}; $\nu_{(C=N\ st)}$ 1,576 cm^{-1}; $\nu_{(C=C\ st)}$ 1,533 cm^{-1}; $\nu_{(C\text{-}F\ st,\ CF3)}$ 1378, 1316 cm^{-1}; out-of-plane asymmetric $\nu_{(C\text{-}F\ st)}$ 1,179 cm^{-1} ; in-plane $\nu_{(C\text{-}H\ bend)}$ 1,127 cm^{-1} (**Figures S1a, ESI**); MS MALDI-TOF: m/z: 1096. 23 [**Eu1**]$^+$; 1119.05 for [**Eu1**+Na]$^+$, 969.94 [(Eu(btfa)$_2$(FurTerPy)+K+MeOH+H_2O]$^+$ **Figure S5, ESI**. UV-vis [CH_2Cl_2, λ/nm (ε/ M^{-1}cm^{-1}); 252 (4271), 296 (5705), 321 (6762).

[Eu(btfa)$_3$(ThioTerPy)] (Eu2): Eu2 was prepared by the same general synthetic route as **Eu1.** Analysis calculated for $C_{51}H_{33}EuF_9N_3O_6$, C, 55.35; H, 3.01; N, 3.80; observed C, 55.40; H, 3.08; N, 3.76%. FTIR (solid; cm^{-1}): $\nu_{(ar\ C\text{-}H\ st)}$ 3060 cm^{-1}; $\nu_{(C=O\ st)}$ 1,626 cm^{-1}; $\nu_{(C=N\ st)}$ 1,580 cm^{-1}; $\nu_{(C=C\ st)}$ 1,538 cm^{-1}; $\nu_{(C\text{-}F\ st,\ CF3)}$ 1370, 1318 cm^{-1}; out-of-plane asymmetric $\nu_{(C\text{-}F\ st)}$ 1,182 cm^{-1}; in-plane $\nu_{(C\text{-}H\ bend)}$ 1,122 cm^{-1} (**Figure S1b, ESI**); MS (MALDI-TOF): m/z: 840.57 [(Eu(btfa)($C_6H_5COCH_3$)(ThioTerPy)+K]$^+$, 1137.22 for [**Eu2**+Na+H]$^+$ **Figure S6, ESI**. UV-vis [CH_2Cl_2, λ/nm (ε/ M^{-1}cm^{-1}); 253 (5725), 297 (7084), 322 (8761) (6762).

[Eu(btfa)$_3$(NapTerPy)] (Eu3): Eu3 was prepared by the same synthetic route as **Eu1** and **Eu2.** Analysis calculated for $C_{51}H_{33}EuF_9N_3O_6$, C, 55.35; H, 3.01; N, 3.80; observed C, 55.40; H, 3.08; N, 3.76%. FTIR (solid; cm^{-1}): $\nu_{(ar\ C\text{-}H\ st)}$ 3060 cm^{-1}; $\nu_{(C=O\ st)}$ 1,626 cm^{-1}; $\nu_{(C=N\ st)}$ 1,578 cm^{-1}; $\nu_{(C=C\ st)}$ 1,536 cm^{-1}; $\nu_{(C\text{-}F\ st,\ CF3)}$ 1393, 1321 cm^{-1}; out-of-plane asymmetric ν(C-F st) 1,178 cm^{-1}; in-plane $\nu_{(C\text{-}H\ bend)}$ 1,122 cm^{-1} (**Figure S1c, ESI**); MS (MALDI-TOF): m/z: 1225.93 [**Eu3**+K+MeOH]$^+$, 1058.88 for [(Eu(btfa)$_2$(C_2HF_3O)(NapTerPy)-H]$^+$**Eu2**+Na+H]$^+$, 1099.65 for [(Eu(btfa)$_2$($C_6H_5COCH_3$)(NapTerPy)+K]$^+$ **Figure S7, ESI**.UV-vis [CH_2Cl_2, λ/nm (ε/ M^{-1}cm^{-1}); 255 (9631), 267 (9348) 285 (8308), 317 (6988).

Spectroscopic Measurements and Determination of Photophysical Parameters

Spectroscopic measurements of **Eu1**, **Eu2** and **Eu3** including optical absorption, excitation, emission spectra, decay profiles and absolute PLQY values were obtained at room temperature; details of the measurements have been reported previously.[3, 39] Optical absorption spectra were obtained using Varian Cary 5000 UV-Visible-NIR spectrophotometer while excitation, emission spectra and decay profiles were recorded on an Edinburgh FS5 fluorimeter. The absolute PLQY (Q_L^{Eu}) were determined using a calibrated integrating sphere on a C-9920-02 from the Hamamatsu Photonic instrument. Photophysical parameters such as the J-O parameters (Ω_2 and Ω_4), radiative (A_{Rad}), non-radiative (A_{NRad})

decay rates, natural radiative lifetime (τ_{Rad}), intrinsic quantum yield (Q_{Eu}^{Eu}) and sensitization efficiency (η_{Sen}) were calculated by applying the following set of equations and details of the calculations are reported elsewhere. [5, 40]

$$\Omega_{\lambda}^{\exp} = \frac{3\hbar A_{Rad}\left[{}^5D_0 \rightarrow {}^7F_J\right]}{32e^2\pi^3\chi\nu\left[{}^5D_0 \rightarrow {}^7F_J\right]^3\left|\left\langle {}^5D_0\left\|U^{(\lambda)}\right\|{}^7F_J\right\rangle\right|^2} \quad \text{Eq. 1}$$

$$A_{Rad} = \sum_{J=0}^{4} A_{Rad}\left[{}^5D_0 \rightarrow {}^7F_J\right] \quad \text{Eq. 2}$$

$$A_{Rad}\left[{}^5D_0 \rightarrow {}^7F_J\right] = \frac{\nu\left[{}^5D_0 \rightarrow {}^7F_1\right]}{\nu\left[{}^5D_0 \rightarrow {}^7F_J\right]} \times \frac{A\left[{}^5D_0 \rightarrow {}^7F_J\right]}{A\left[{}^5D_0 \rightarrow {}^7F_1\right]} A_{Rad}\left[{}^5D_0 \rightarrow {}^7F_1\right] \quad \text{Eq. 3}$$

$$A_{tot} = \frac{1}{\tau_{obs}} = A_{Rad} + A_{NRad} \quad \text{Eq. 4}$$

$$\tau_R = 1 \Big/ A_{Rad} \quad \text{Eq. 1}$$

$$Q_{Eu}^{Eu} = \frac{\tau_{obs}}{\tau_{Rad}} = \frac{A_{Rad}}{A_{Rad} + A_{NRad}} \quad \text{Eq. 2}$$

$$\eta_{sen} = \frac{Q_{Eu}^{L}}{Q_{Eu}^{Eu}} \quad \text{Eq. 7}$$

Details of the determination of ground state geometry, singlet (S) and triplet State (T) energy levels, methodology of modelling energy transfer (ET) mechanism and ET rates, A_{Rad}, and A_{NRad} decay rates and theoretical PLQY of the sensitized PL is detailed in the ESI. Fabrication of OLEDs and assessments of their EL performance is also summarized in the ESI.

Results and Discussion

The new asymmetric nonacoordinated OEuCs (**Eu1** – **Eu3**) were synthesized by a simple and established two-step method.[15, 41] The isolated OEuCs were characterized by elemental analysis, mass spectrometry and FTIR spectroscopy and their composition agreed with the proposed chemical structures and stoichiometry, as shown in **Chart 1b**. Lower C=N stretching frequency is observed in all the complexes compared to their free ligands implying coordination of the ligand through nitrogen to the Eu(III) (**Figure S1, ESI**), for instance, $\nu_{(C=N\ st)}$ 1,576 cm^{-1}, 1,580 cm^{-1}, 1,578 cm^{-1}, for **Eu1**, **Eu2** and **Eu3**, respectively. The complexes proved surprisingly difficult to crystallize. Despite our rigorous efforts with repeated crystallization by employing a wide range of solvents/mixed solvents, we were unable to obtain single crystals suitable for X-ray diffraction (XRD) studies. It was against this

backdrop that we turned our attention to determine the structure by theoretical means employing the DFT method. Moreover, the structural information obtained through DFT calculations has the same degree of accuracy as determined by the SC-XRD with an overall root mean square deviation (RMSD) value of the coordination sphere as low as 0.17 Å.[15] It is also important to emphasize that it is necessary to theoretically determine the ground state geometry of the material in question to predict the electronic spectrum, energy levels [S and T] and finally the mechanism of intramolecular energy transfer (IET) for the sensitized PL together with rates of ET that are involved in IET. The ground state geometry of the **Eu1**, **Eu2**, and **Eu3** was calculated by employing the PBE1PBE/TZVP/MWB52 DFT method, the resultant structures are shown in **Figure 1** while the corresponding spherical coordinates of each atom directly coordinated to the central Eu(III) ion are listed in **Table S1 – S3, ESI**.

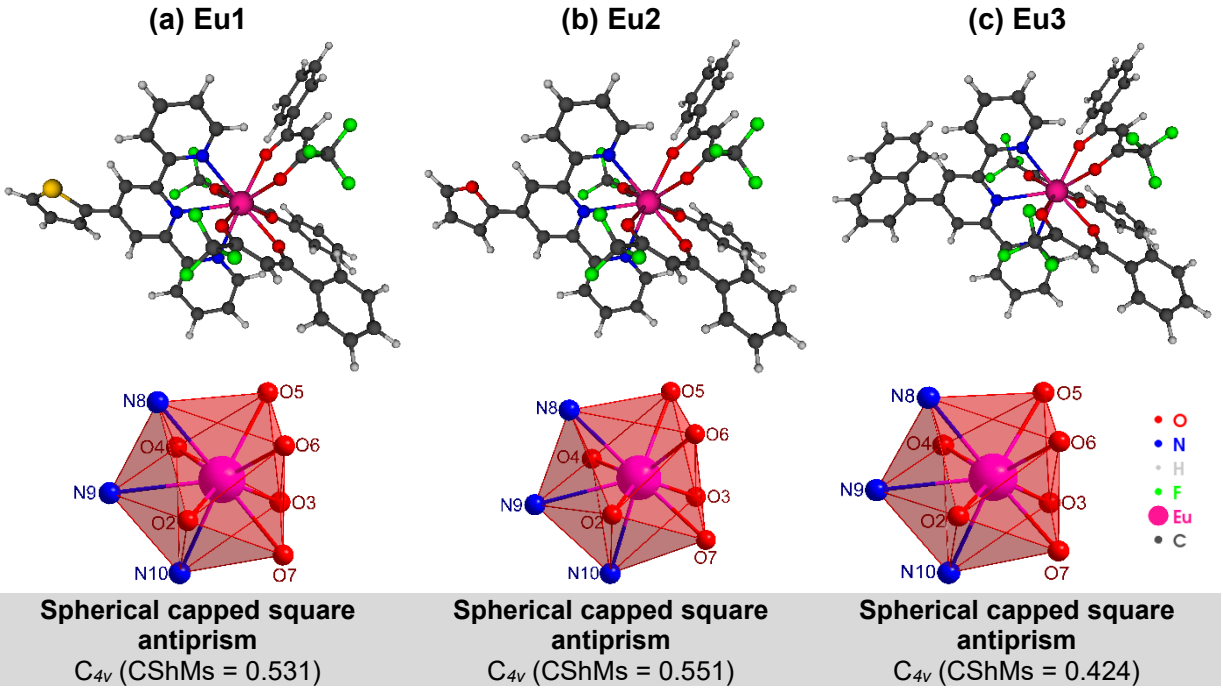

Spherical capped square antiprism C_{4v} (CShMs = 0.531)	**Spherical capped square antiprism** C_{4v} (CShMs = 0.551)	**Spherical capped square antiprism** C_{4v} (CShMs = 0.424)

Figure 1: The ground state molecular structure of the asymmetric nonacoordinated complexes and their coordination geometry calculated with the PBE1PBE/TZVP/MWB52 method (a) **Eu1**, (b) **Eu2** and (c) **Eu3**.

As noted in our previous studies[39] the DFT methods tend to marginally overestimate the Eu-N bond lengths compared to experimentally observed distances. A similar observation is also noted for the three studied complexes exhibiting $(Eu\text{-}N)_{Avg.}$ bond distances of approximately 2.67 Å, while the average $(Eu\text{-}O)_{Avg.}$ bond distances were found to be approximately 2.43 Å. It is worth mentioning that both Eu-N and Eu-O distances closely align with those calculated in previous studies by applying DFT methods. The comparison in terms of RMSD involving the geometry of different Eu(III) complexes further revealed that the DFT geometries were in excellent agreement with those obtained from SC-XRD and thus

is useful to elucidate the symmetry of the coordination polyhedron around Eu(III). The coordination environment of the studied complexes is nonacoordinate (N_3O_6), consisting of six oxygen (O) atoms from btfa ligands and three nitrogen (N) atoms from the TerPy ligand (see **Figure 1**). The coordination polyhedron of the complexes is described as a distorted spherical capped square antiprism with symmetry idealized as C_{4v} (**Table S4, ESI**). This description was achieved from the DFT geometry together with the SHAPE program,[42, 43] which compares the continuous shape measures (CShMs) for a given coordination geometry relative to the vertices of an ideal reference polyhedron. A low-symmetry chemical environment around the Eu(III) ion suggests significant values for certain spectroscopic properties, such as the intensity parameters.

Analysis and Discussion of Experimental and Theoretical Photophysical Properties

To understand the light absorbing abilities of the present OEuCs, the optical absorption spectra were measured in dilute dichloromethane (DCM; CH_2Cl_2) solution (**Figure 2a**) together with the free TerPy ligands (separate overlapping electronic spectra **Figure S8,** is included in **ESI**). As can be seen from **Figure 2a**, the electronic absorption spectra of **Eu1, Eu2, and Eu3** show combined absorption bands of the primary btfa and ancillary TerPy ligands in DCM solution with a λ_{abs}^{max} at 322 nm (molar absorptivity (ε) = 10247 $M^{-1}cm^{-1}$) for **Eu1**, 322 nm (ε =13234 $M^{-1}cm^{-1}$) for **Eu2** and 255 nm (ε =14470 $M^{-1}cm^{-1}$) and 318 nm (ε =10465 $M^{-1}cm^{-1}$) for **Eu3**, respectively. The high ε values imply that the new OEuCs have good light absorbing capability and thus strongly emitting complexes should be obtained. To underpin the results of absorption spectroscopy and to navigate the role of btfa and TerPy ligands in the light absorption phenomenon of the present OEuCs, we calculated the absorption spectra by the TD-DFT method (**Figure 2b**), where the solvent effect DCM was implicitly considered in the calculations. It is possible that the λ_{abs}^{max} value for all calculated spectra was slightly underestimated and this behaviour has previously been documented in research conducted by our group, even by applying different density functionals in the TD-DFT approach.[31, 39, 44] In this context, the results attest that the accurate determination of λ_{abs}^{max} is one of the main shortcomings of the TD-DFT method. Nevertheless, an examination of the theoretical spectra reveals that the positions of the absorption bands most shifted to longer wavelengths are consistent with the experimental observations. This alignment is evident since the **Eu1** and **Eu2** complexes exhibited bands at nearly identical wavelengths (281 and 283 nm, respectively). In contrast, the absorption peak corresponding to **Eu3** exhibited a shift towards shorter wavelengths (277 nm).

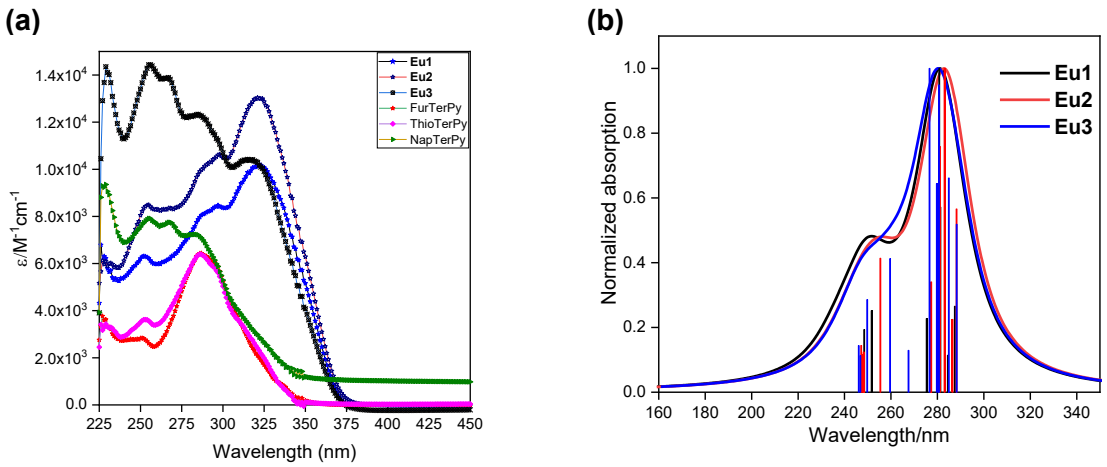

Figure 2: (a) Electronic absorption spectra of Fur-TerPy, Thio-TerPy, NapTerPy, **Eu1**, **Eu2** and **Eu3** in CH_2Cl_2 (1×10^{-5} M). (b) Theoretical absorption spectra predicted by the TD-DFT method (with the implicit effect of solvent) for **Eu1**, **Eu2** and **Eu3** from the geometry calculated at the PBE1PBE/TZVP/MBW52 level of theory.

In addition, the TD-DFT method proved to be an important tool for identifying the subunit in the molecule most relevant for a given absorption band in these studies. In this way, to gain insight into the nature of the most relevant transitions, an analysis of natural transition orbitals (NTOs) was performed based on the information extracted from the singlet excited states calculated using the CAM-B3LYP/TZVP/MWB52 method (**Figure 3**). This analysis offers a straightforward interpretation of the transition density between the ground state and a specific excited state.[45] As can be seen in **Figure 3**, the most intense bands of the **Eu1** and **Eu2** complexes have the contribution from electronic transitions involving molecular orbitals (MOs) located at the primary btfa and ancillary ligands (FurTerPy and ThioTerPy). Interestingly, the main electronic transitions for **Eu3** are derived primarily from the NapTerPy ligand and mask the btfa absorption. The result further corroborates the experimental absorption spectrum of **Eu3** and explains the blue shift in the λ_{abs}^{max} of **Eu3** compared to **Eu1** and **Eu1**.

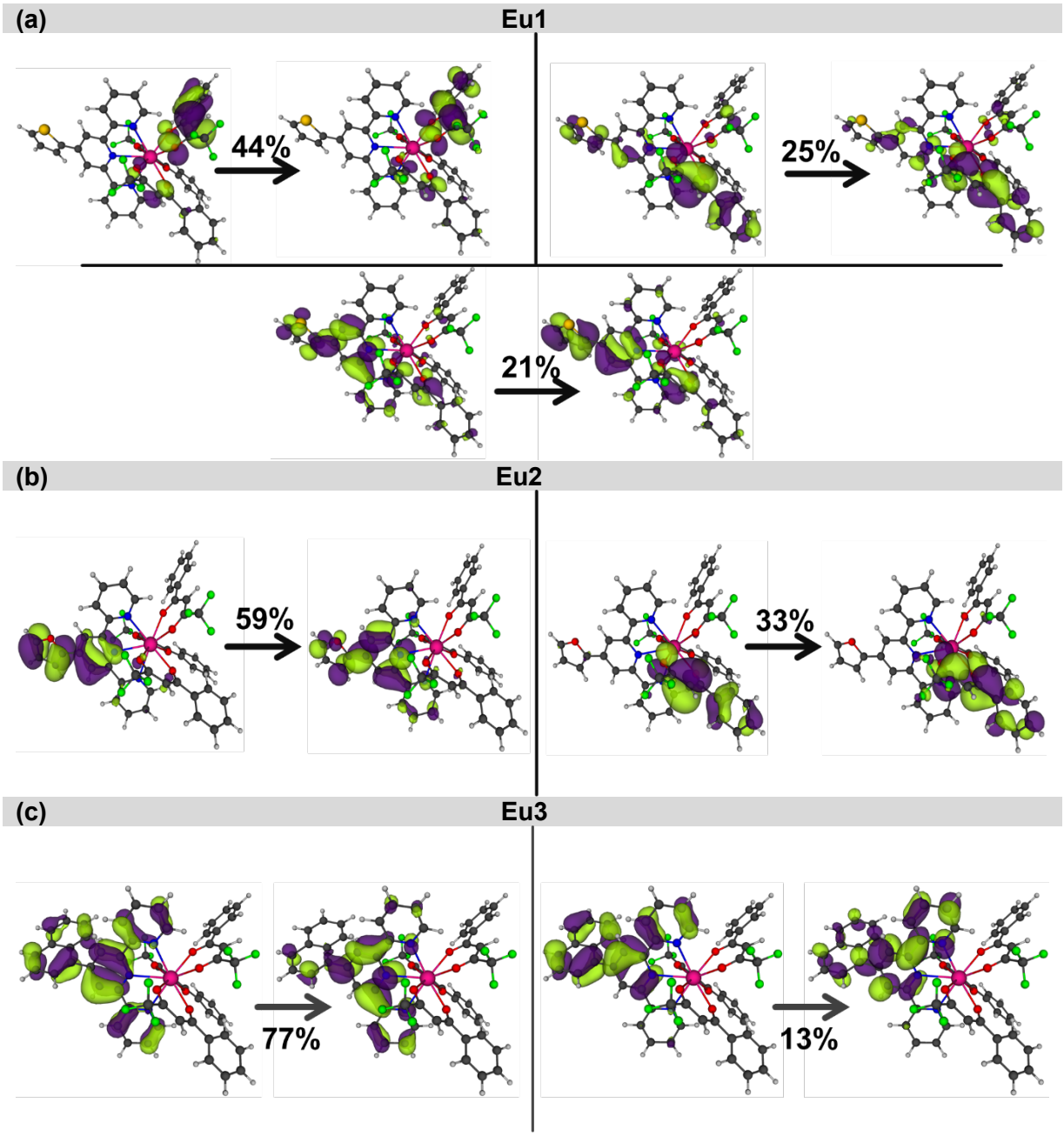

Figure 3: Picture of the NTO mainly contributing to the most intense bands of (**a**) **Eu1**, (**b**) **Eu2**, and (**c**) **Eu3** calculated using CAM-B3LYP/TZVP/MWB52 (DCM), where the percentages indicate the contribution of each transition to the singlet excited state corresponding to the respective absorption.

The steady-state emission spectra of OEuCs were obtained at λ_{abs}^{max} in the solid-state and are shown in **Figure 4** and individual excitation and emission spectra together with the absorption spectrum are also included in the supporting information (**Figure S9, ESI**). The excitation spectra in each case exhibit a composite broad band in the UV region that resembles the absorption spectra. Besides, the excitation spectra also displayed faint intra-configurational f – f transitions at 463 nm and ($^5D_2 \leftarrow {}^7F_{0,4}$) and 533 nm ($^5D_{1,2} \leftarrow {}^7F_{1,4}$) for **Eu1**

and **Eu2** and unnoticeable transitions for **Eu3**. The presence of weak intra-configurational f – f transitions signifies the sensitisation of the europium PL by the well-known antenna mechanism.[36, 46] Important PL data extracted from the steady-state emission spectra of **Eu1** – **Eu3** that include barycentre of the emission transitions, the emission intensity of the transitions and % contribution of each transition relative to magnetic-dipole (MD) $^5D_0 \rightarrow {}^7F_1$ transition are listed in **Table 1**. The steady-state emission spectra of **Eu1** – **Eu3** exhibit five well-resolved inherent emission transitions typical for Eu(III) in the region between 500 and 750 nm.[41] The prevailing nature of the induced electric-dipole (ED) $^5D_0 \rightarrow {}^7F_2$ emission transitions (80 – 85% of the total integrated emission intensity) over the other four transitions especially MD $^5D_0 \rightarrow {}^7F_1$ transition signifies the dominance of the forced electric dipole (FED) and dynamic coupling (DC) mechanism in the emission process of **Eu1** – **Eu3**.

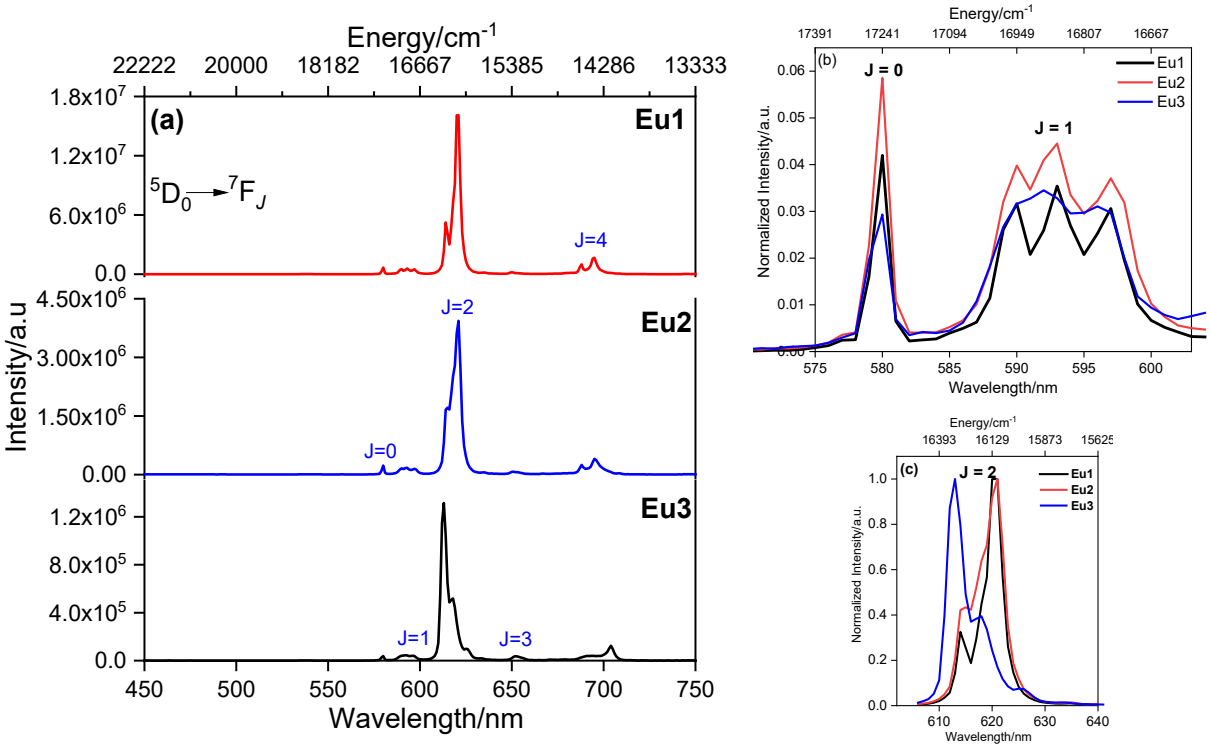

Figure 4: (a) Steady-state emission spectra of solid **Eu1**, **Eu2** and **Eu3**. (b) Magnified view of the emission spectra of **Eu1**, **Eu2** and **Eu3** in the region between 575 nm and 602 nm and (c) Magnified view of the emission spectra of **Eu1**, **Eu2** and **Eu3** in the region between 605 nm and 640 nm.

Moreover, this transition is also accountable to brilliant red emission with the International Commission on Illumination $(CIE)_{x,y}$ colour coordinates $(0.674, 0.321)_{Eu1}$, $(0.658, 0.318)_{Eu2}$ and $(0.671, 0.325)_{Eu3}$ (**Figure S10, ESI**), which is equivalent to NTSC CIE colour coordinate for red emission i.e., (0.67, 0.33). Thus, the synthesized OEuCs could be potential candidate for the manufacture of white-OLEDs by RGB method and as patches in wound dressings that could be useful for wound healing and skin rejuvenation.[47] The intensity ratio (R_{21}),

which is a ratio of ED $^5D_0 \rightarrow {}^7F_2$ to MD $^5D_0 \rightarrow {}^7F_1$ emission transitions is calculated and listed in **Table 1**. The higher R_{21} values of the three OEuCs under discussion indicate that Eu(III) is coordinated in a site without an inversion centre and symmetry around it is lower[48] and this is in agreement with the CShMs values. Interestingly, the R_{21} values (**Table 1**) of the three OEuCs are close suggesting similar symmetries i.e., within the boundary of the same asymmetric environment. Furthermore, R_{21} values are higher than that of analogues [Eu(btfa)$_3$(Ph-terPy)] (R_{21} = 15.74)[31] and point that the symmetry of OEuCs is more asymmetric but remains within the limit of the same asymmetric environment. In order to obtain a greater insight, excited state lifetime (τ_{obs}) of $^5D_0$ emitting state was determined by fitting the PL decay curves (**Figure S11 – S13, ESI**) monitored within the induced ED $^5D_0 \rightarrow {}^7F_2$ emission transition and data obtained are shown in **Table 1**. The decay profiles of **Eu1** – **Eu3** fit very well mono-exponential fitting (χ^2= 1.030 – 1.073) and confirm the presence of a single dominant emitting species. The excited state lifetime of the present OEuCs falls in the µs regime typical of ternary europium tris(β-diketonate) complexes with similar τ_{obs} = 699.98 ± 1.34 µs for **Eu1**, τ_{obs} = 692.66 ± 1.41 µs for **Eu2** and τ_{obs} = 659.87 ± 0.58 µs for **Eu3**, respectively. The results further agreed with the solid-state absolute PLQY which are similar i.e., Q_L^{Eu} = 59.30% for **Eu1**, 59.74% for **Eu2** and 61.48% for **Eu3**, respectively (**Table 1**) and marginally higher than [Eu(btfa)$_3$(Ph-terPy)] (Q_L^{Eu} = 54.90%). Finally, the J-O Ω_2 and Ω_4 is calculated and is a handy tool for evaluating behaviour of the OLnCs. For instance, Ω_2 provides information about the probability of FED transitions and symmetry of the coordination polyhedron while Ω_4 furnishes the information regarding the presence and absence of long-range effects (hydrogen bonding, π-π stacking, etc).[40, 49] As expected, the asymmetric OEuCs exhibited large Ω_2 values that correlate well with R_{21}.

Table 1: Room temperature photophysical properties of **Eu1** – **Eu3** in the solid-state.

Properties	Eu1	Eu2	Eu3
$^5D_0 \rightarrow {}^7F_0$	17247.92 cm^{-1} (1.00 %)	17247.70 cm^{-1} (1.08 %)	17251.54 cm^{-1} (0.77 %)
$^5D_0 \rightarrow {}^7F_1$	16864.12 cm^{-1}	16864.19 cm^{-1}	16869.03 cm^{-1}
$^5D_0 \rightarrow {}^7F_2$	16142.94 cm^{-1} (85.18 %)	16150.25 cm^{-1} (79.97 %)	16242.10 cm^{-1} (83.71 %)
$^5D_0 \rightarrow {}^7F_3$	15360.09 cm^{-1} (1.13%)	1 5344.97 cm^{-1} (1.76%)	15324.91 cm^{-1} (3.09%)
$^5D_0 \rightarrow {}^7F_4$	14425.94 cm^{-1} (12.67%)	14418.39 cm^{-1} (12.27%)	14325.71 cm^{-1} (12.47%)
FWHM of $^5D_0 \rightarrow {}^7F_2$ (nm)	3.77	5.77	3.76
Intensity Ratio (R_{21})[a]	17.64	16.29	17.33
CIE Coordinates	0.674, 0.321	0.658, 0.318	0.665, 0.328
τ_{obs} (µs)	699.98 ± 1.34 (χ^2= 1.073)	692.66 ± 1.41 (χ^2= 1.073)	659.87 ± 0.58 (χ^2= 1.030)
Ω_2 (× 10^{-20} cm^2)[b]	31.50 [31.50]	29.07 [29.08]	30.27 [30.27]
Ω_4 (× 10^{-20} cm^2)[b]	9.98 [10.00]	9.78 [9.77]	10.34 [10.35]
A_{Rad} (s^{-1})[c]	1171.97 [1146.23]	1081.68 [1069.97]	1150.43 [1114.58]
A_{NRad} (s^{-1})[c]	258.65 [282.38]	363.40 [373.74]	364.72 [400.87]
τ_R (µs)[d]	853.26	924.48	869.24
Q_{Eu}^{Eu} (%)[e]	81.92 [80.23]	79.81 [74.11]	75.93 [73.55]
Q_L^{Eu} (%)	59.30 [56.22]	59.74 [55.61]	61.48 [58.08]
η_{Sen} (%)[f]	72.38 [70.07]	74.85 [75.04]	80.96 [78.97]

Values in the square bracket are % contribution relative to $^5D_0 \rightarrow {}^7F_1$ MD transition; [a]Ratio of the integrated intensity of the induced electric dipole (ED) $^5D_0 \rightarrow {}^7F_2$ to the $^5D_0 \rightarrow {}^7F_1$ MD transition; [b]Ω_2 and Ω_4 were calculated by applying equation 1 and 2; [c]A_{Rad} and A_{NRad} were calculated by applying equation 2 – 4, ESI; [d]τ_R was calculated by applying equation 5, ESI; [e]Q_{Eu}^{Eu} was calculated by applying equation 6, ESI; [f]$\eta_{Sen}$was calculated by applying equation 7, ESI

Analysis and Discussion of the IET Mechanism

By utilizing the information extracted from the TD-DFT results, it is also possible to gain a deeper understanding of the IET process of the three complexes by applying the LUMPAC software.[35] The energy of the lowest singlet (S_1) and triplet (T_1) excited states along with their corresponding distance (R_L) from the energy donor to the acceptor centre and the most relevant electronic transitions that compose S_1 and T_1 states are depicted in **Table 2**. Although NapTerPy in **Eu3** possesses both the larger structural extension and greater π-electron conjugation, the R_L values of the complexes are comparable (**Table 2**). Furthermore, it is also worth highlighting that the energy of S_1 and T_1 remained relatively unchanged across the three complexes despite the structural modifications introduced at the 4' position of the TerPy ancillary ligands. Consequently, we expect that the impact of the ancillary ligand on the IET process of the three complexes will be similar and thus would result in similar Q_L^{Eu}, which indeed is the case. A possible explanation for this observation could be found by analysing the MOs that are involved in electronic transitions of the S_1 and T_1 states (**Table 2**). Scrutiny of MOs further revealed that they are located on both the btfa and TerPy ligands (**Figure S14, ESI**). In addition, the constitution of the MOs across the complexes is also identical. By considering the HOMO-1 and LUMO orbitals, it becomes very clear that the HOMO-1 exhibits contributions from orbitals centred on one of the primary btfa ligands, while LUMO contributions involve orbitals from the atoms of the ancillary TerPy ligand (**Figure S14, ESI**).

The S_1 and T_1 energy of each complex, along with the corresponding distance R_L, were utilized in Malta's model[50] to calculate the ET rates for two excited states with the help of LUMPAC. The rates calculated for the **Eu1, Eu2** and **Eu3** complexes relating the S_1 and T_1 and various excited levels of Eu(III) ($^5D_0$, $^5D_1$, $^5D_2$, $^5D_3$, $^5D_4$, $^5L_6$, $^5L_7$, $^5G_2$, $^5G_3$, $^5G_5$, and $^5G_6$) are shown in **Table 3** and **Table S5** and **Table S6, ESI**, where a total of 90 rates were estimated for each complex, distributed as 30 for Coulombic interaction (CI), 30 for Exchange (Ex.) mechanism and 30 for backward ET. The ET rates related to the CI mechanism were quantified using the FED intensity parameters (Ω_λ^{FED}) provided by the *QDC* model[51] (see **Tables S7 – S9**, **ESI**) developed by one of us and implemented in LUMPAC.[35] The emission of the Eu(III) is typically dominated by the DC mechanism, which is a function of the polarizabilities of the atoms belonging to the coordination polyhedron of the complexes. This observation is based on the larger value of the Ω_λ^{DC} parameter in comparison to Ω_λ^{FED}, as can be seen in **Table S7 – Table S9**, **ESI**, for all complexes under investigation. As noted by us[2, 15, 21, 39] and other research groups,[52, 53, 54] the most significant ET pathways promoting PL in the OEuCs involves the $T_1 \rightarrow {}^5D_0$ and $T_1 \rightarrow {}^5D_1$ ligand-metal transitions. This fact highlights the significant role played by the T states of the ligands in the ET process. The highest values related to the $^7F_0 \rightarrow {}^5D_1$ and $^7F_1 \rightarrow {}^5D_0$ excitations (around 10^7

s^{-1} for all complexes) suggest that the Ex. mechanism is the principal pathway responsible for the excitation of the Eu(III) ion. When the ET rates for the S_1 states are considered, the highest rates are around 10^5 s^{-1}, which are associated with the $^7F_1 \rightarrow {}^5G_2$ and $^7F_1 \rightarrow {}^5G_3$ transitions, further reinforcing the importance attributed to the triplet states. The magnitudes of the rates are very similar to those found in a recent study conducted by us, in which the theoretical modelling of ET for the complexes [Eu(btfa)$_3$(Ph-terPy)] and [Eu(NTA)$_3$(Ph-terPy)] was performed.[31]

Table 2: Energy of the lowest singlet and triplet excited states, electronic transitions for the respective excited states, and respective distance from energy donor to acceptor centre (R_L) of **Eu1**, **Eu2** and **Eu3** estimated using the CAM-B3LYP/TZVP/MWB52 (DCM) result with the help of LUMPAC.

Compound	State	Energy/cm^{-1}	R_L/Å	Major Contribution	Total
Eu1	S_1	33481.30	4.48	HOMO-12→LUMO+1 (44.14%) HOMO-12→LUMO+4 (14.10%) HOMO-14→LUMO+1 (10.25%)	68.48%
	T_1	22822.90	4.50	HOMO→LUMO+2 (32.75%) HOMO→LUMO+1 (12.49%) HOMO→LUMO+4 (10.34%) HOMO-1→LUMO+2 (9.95%)	65.53%
Eu2	S_1	33470.80	4.43	HOMO-11→LUMO+1 (43.00%) HOMO-11→LUMO+4 (13.05%) HOMO-13→LUMO+1 (10.23%)	66.28%
	T_1	22825.60	4.46	HOMO-2→LUMO+2 (17.23%) HOMO-1→LUMO+2 (12.69%) HOMO→LUMO+2 (12.36%) HOMO-2→LUMO+1 (9.73%) HOMO-1→LUMO+1 (7.66%) HOMO→LUMO+1 (7.25%) HOMO-2→LUMO+4 (5.49%)	72.41%
Eu3	S_1	33580.60	4.61	HOMO-12→LUMO+1 (26.01%) HOMO-12→LUMO+4 (20.10%) HOMO-12→LUMO+2 (13.21%) HOMO-12→LUMO (7.11%)	66.43%
	T_1	22746.30	4.51	HOMO-1→LUMO+1 (53.55%) HOMO-1→LUMO+4 (13.60%) HOMO-1→LUMO+2 (8.87%) HOMO-1→LUMO (5.03%)	81.05%

Figure 5 shows a postulated energy level diagram that illustrates the most important channels involved in the ligand-to-Eu(III) ET processes for all three complexes. Furthermore, as the MO analysis revealed the contribution of the β-diketonate and neutral ancillary TerPy

ligands to the composition of the S_1 and T_1 states, only these two states were considered in the Jablonski diagram. From the Eu(III) perspective, all excited levels contained in the electronic excitations listed in **Table 3, Table S5** and **Table S6, ESI** were taken into account in the ET process. When the η_{Sen} value is lower than 100%, probably there is an eventual pathway that depopulates T_1. When the T_1 is situated below the $^5D_0$ and $^5D_1$ states, the possibility of a significantly large ET rate from $^5D_0$ and $^5D_1$ to T_1 increases, leading to a decrease in η_{Sen}. However, this is not the case for the complexes under consideration. To reproduce the experimental η_{Sen} and Q_{Eu}^{L} of the complexes,[44] the ligand decay rates related to the $S_1 \rightarrow S_0$, $S_1 \rightarrow T_1$, and $T_1 \rightarrow S_0$ transition were adjusted, following a method already applied in our previous work.[31, 39, 55]

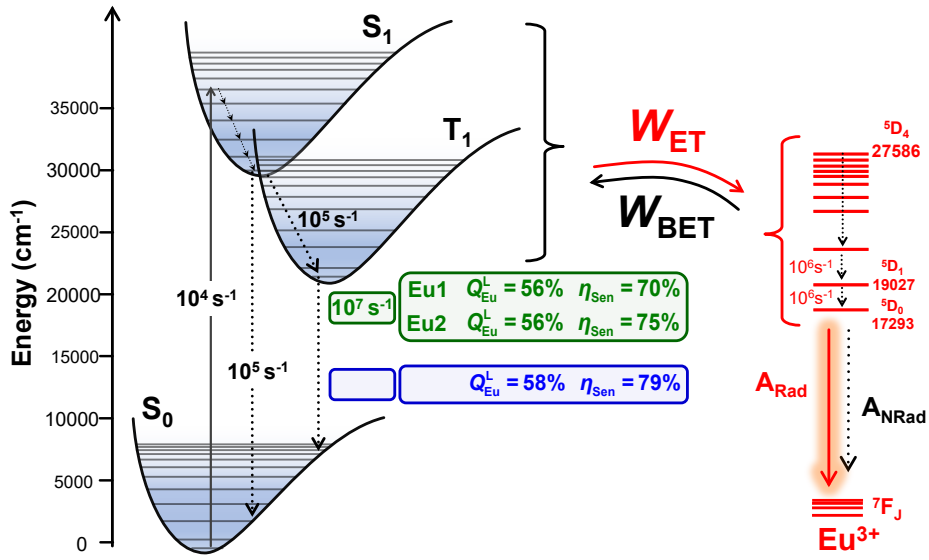

Figure 5: Representative Jablonski diagram illustrating the ligand and Eu(III) states involved in the process of energy transfer of the **Eu1**, **Eu2**, and **Eu3** complexes.

The close resemblance of the experimental Q_L^{Eu} values (see **Table 1**) indicates a relatively minor structural difference among the complexes. However, even in this context, the η_{Sen} values reflect more significant differences to those observed for Q_L^{Eu}. In the process of adjusting the rates, these facts were contemplated, and the adjusted values for the decay rates of the $S_1 \rightarrow S_0$, $S_1 \rightarrow T_1$, and $T_1 \rightarrow S_0$ transitions are presented in **Figure 5**. The same set of decay rates for **Eu1** (Q_L^{Eu}: 59 % *vs.* 56 %; η_{Sen}: 72 % *vs.* 70 %) and **Eu2** (Q_L^{Eu}: 60 % *vs.* 56 %; η_{Sen}: 75 % *vs.* 75 %) complexes resulted in the values of quantum yield and sensitization efficiency that closely matched those obtained experimentally. In the case of **Eu3** (Q_L^{Eu}: 58 % *vs.* 61 %; η_{Sen}: 79 % *vs.* 81 %), the highest value of η_{Sen} suggests that the depopulation efficiency of the T_1 state in **Eu3** is lower compared to the other two complexes, as indicated by the adjusted rate related to the $T_1 \rightarrow S_0$ transition, which is equal to 10^5 s^{-1}.

Table 3: Energy transfer rates quantified with LUMPAC for **Eu3** using Malta's model[50] based on the TD-DFT CAM-B3LYP/TZVPPD/MWB52 results with the implicit effect of the DCM solvent included in the calculations. The $^5D_0 \leftarrow {}^7F_0$ transition was included in the calculations by means of a *J*-mixing of 5% involving the $^7F_0$ and $^7F_2$ states.

	Donor	Acceptor	W_{ET}^{CI} (s^{-1})	W_{ET}^{EX} (s^{-1})	W_{BET} (s^{-1})
Eu3	S_1	$^7F_0 \rightarrow {}^5D_0$	4.07×10^{-2}	0.0	4.85×10^{-36}
		$^7F_0 \rightarrow {}^5D_1$	0.0	4.35×10^{1}	2.11×10^{-29}
		$^7F_0 \rightarrow {}^5L_6$	1.16×10^{2}	0.0	7.43×10^{-16}
		$^7F_0 \rightarrow {}^5G_6$	1.16×10^{2}	0.0	6.92×10^{-13}
		$^7F_0 \rightarrow {}^5D_4$	9.49×10^{3}	0.0	3.10×10^{-9}
		$^7F_1 \rightarrow {}^5D_0$	0.0	8.62×10^{0}	1.03×10^{-33}
		$^7F_1 \rightarrow {}^5D_1$	7.31×10^{1}	2.31×10^{-2}	3.56×10^{-29}
		$^7F_1 \rightarrow {}^5D_2$	0.0	1.65×10^{2}	1.05×10^{-23}
		$^7F_1 \rightarrow {}^5D_3$	2.07×10^{4}	0.0	1.26×10^{-15}
		$^7F_1 \rightarrow {}^5L_6$	3.57×10^{1}	0.0	2.28×10^{-16}
		$^7F_1 \rightarrow {}^5L_7$	1.76×10^{2}	0.0	1.58×10^{-13}
		$^7F_1 \rightarrow {}^5G_2$	0.0	2.31×10^{5}	2.46×10^{-10}
		$^7F_1 \rightarrow {}^5G_3$	1.17×10^{5}	0.0	3.74×10^{-10}
		$^7F_1 \rightarrow {}^5G_6$	6.45×10^{1}	0.0	3.86×10^{-13}
		$^7F_1 \rightarrow {}^5G_5$	9.16×10^{2}	0.0	5.78×10^{-12}
	T_1	$^7F_0 \rightarrow {}^5D_0$	8.38×10^{-1}	0.0	3.67×10^{-12}
		$^7F_0 \rightarrow {}^5D_1$	0.0	2.44×10^{7}	4.37×10^{-1}
		$^7F_0 \rightarrow {}^5L_6$	2.92×10^{-2}	0.0	6.86×10^{3}
		$^7F_0 \rightarrow {}^5G_6$	3.81×10^{-3}	0.0	8.40×10^{5}
		$^7F_0 \rightarrow {}^5D_4$	9.40×10^{-2}	0.0	1.13×10^{9}
		$^7F_1 \rightarrow {}^5D_0$	0.0	5.69×10^{7}	2.49×10^{-4}
		$^7F_1 \rightarrow {}^5D_1$	1.28×10^{2}	1.29×10^{4}	2.34×10^{-4}
		$^7F_1 \rightarrow {}^5D_2$	0.0	2.83×10^{6}	6.60×10^{3}
		$^7F_1 \rightarrow {}^5D_3$	1.86×10^{1}	0.0	4.17×10^{4}
		$^7F_1 \rightarrow {}^5L_6$	8.95×10^{-3}	0.0	2.10×10^{3}
		$^7F_1 \rightarrow {}^5L_7$	1.01×10^{-2}	0.0	3.36×10^{5}
		$^7F_1 \rightarrow {}^5G_2$	0.0	3.66×10^{6}	1.44×10^{14}
		$^7F_1 \rightarrow {}^5G_3$	4.17×10^{0}	0.0	4.93×10^{8}
		$^7F_1 \rightarrow {}^5G_6$	2.12×10^{-3}	0.0	4.68×10^{5}
		$^7F_1 \rightarrow {}^5G_5$	2.93×10^{-2}	0.0	6.81×10^{6}

Fabrication, Assessments and Discussion of Eu1 – Eu3-based OLEDs

After complete analysis and realizing good PL properties of the complexes (**Eu1** – **Eu3**) and to achieve our goal of producing efficient R-OLEDs within the red emitting OEuCs, we finally tested the complexes as EML within the multilayer OLED and fabricated fifteen single-EML OLEDs (five for each complex) and fifteen double-EML devices (five for each complex). The doping concentration of the OEuCs was modulated to get the maximum EL performance output from the complexes. The designed single-EML OLEDs have a very simple structure as shown in **Figure 6a** and consists of a hole injection layer (HIL) of HAT-CN (6 nm) (dipyrazino[2,3-f:2',3'-h]quinoxaline-2,3,6,7,10,11-hexacarbonitrile), a p-doped hole transport layer (HTL) [0.2 wt% HAT-CN: 4,4'-(cyclohexane-1,1-diyl)bis(N,N-di-p-tolylaniline) (TAPC)

(50 nm)] and an electron transport layer (ETL) (1,3,5-tris(6-(3-(pyridin-3-yl)phenyl)pyridin-2-yl)benzene (Tm3PyP26PyB; 60 nm).

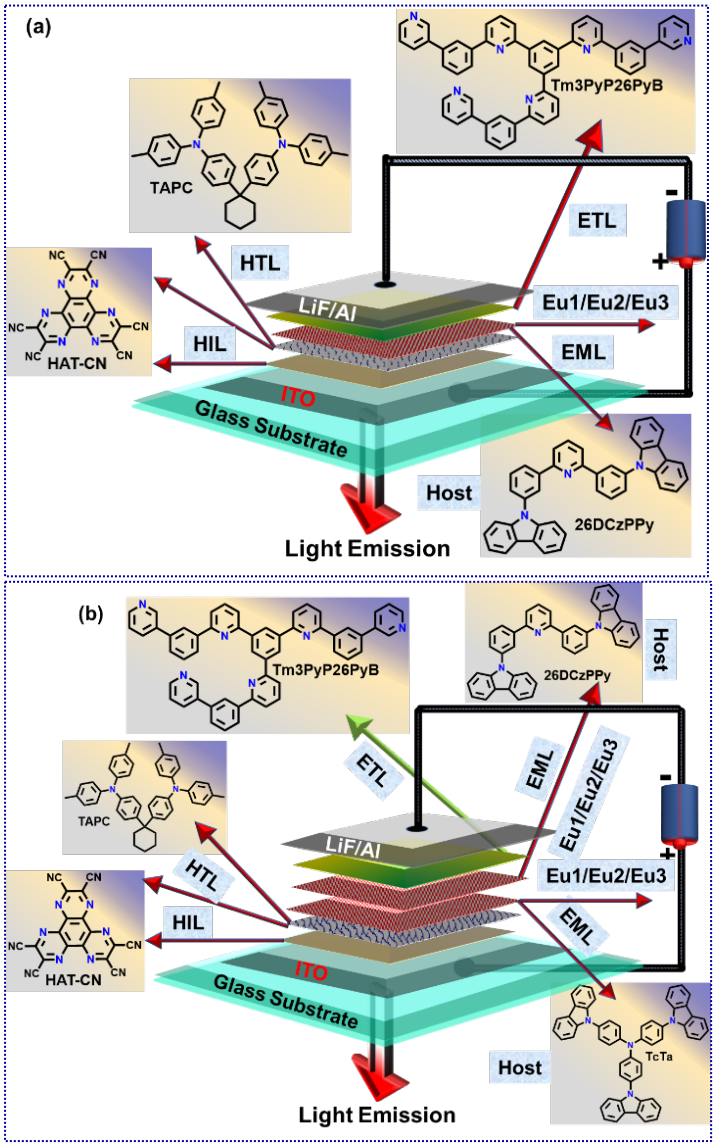

Figure 6: General device configuration of (a) single-EML and (b) double-EML OLED.

The choice of host materials is also very crucial to develop high-performance OLEDs, given the popularity and our own experience, a bipolar material "26DCzPPy" was employed as a host material in the EML (Please see the supporting information for more specific details of device structure). Comparative EL spectra of the best devices and EL spectra of all the devices are shown in **Figure 7** and **Figures S15 – S17, ESI**. The current efficiency and current density curves, together with the *V-B-J* curves for devices are shown in **Figure 8**, and **Figures S18 – S23, ESI**. Key EL performance parameters of all the devices such as brightness (B), maximum current efficiency (η_c), maximum power efficiency (η_p), EQE and CIE colour coordinates and FWHM of the dominant ED $^5D_0 \rightarrow {}^7F_2$ transitions are summarized in **Table 4**. The EL spectra of the single-EML devices of OEuCs exhibit typical

Eu(III) emission in the region between 500 nm and 750 nm with the dominant narrow ED $^5D_0 \rightarrow {}^7F_2$ transitions responsible for the red emission (**Table 4** and **Figures S24 – S26, ESI**) in each device except **Device 1** of **Eu1** and **Eu3** due to the presence of faint host 26DCzPPy emissions. However, as the doping concentration is increased, the intensity of the host emission decreases. This could be attributed to improved Förster long-range ET from the host 26DCzPPy to OEuCs or increased direct carrier trapping process since more and more OEuCs molecules start to participate in the EL processes.[2]

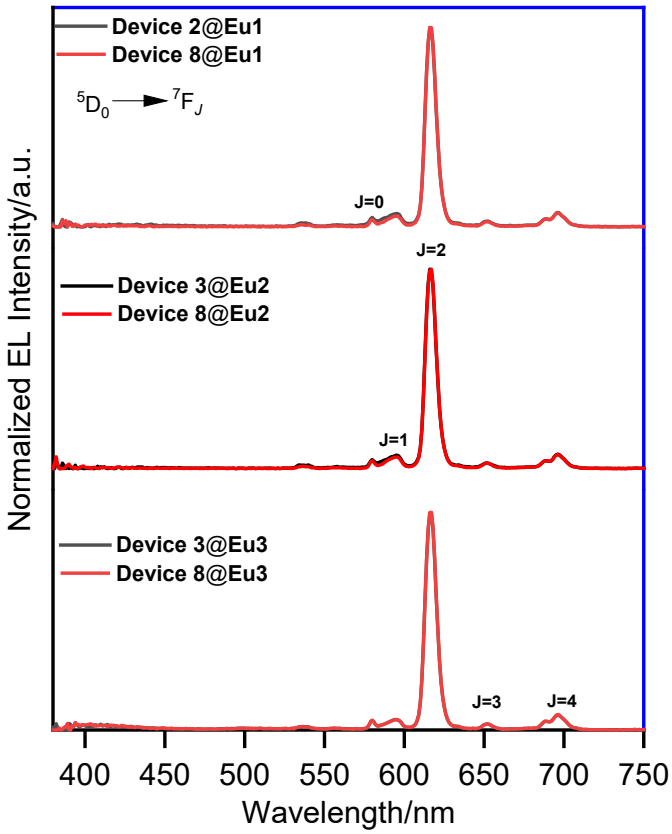

Figure 7: A comparative normalized EL spectra of single-EML and double-EML devices of **Eu1**, **Eu2** and **Eu3** operating at J =10mA/cm^2.

The EL mechanism of the doped device is mainly governed by the two processes, carriers trapping and/or the Förster energy transfer, and dominant character of either mechanism depends on the host as well as the guest in the OLEDs.[56, 57] To ascertain the proposition and to gain the knowledge of dominant EL processes in the devices, we have further determined the photophysical properties of the OEuCs:Host films that include PL spectrum, PLQY and excited state lifetime at the same doping concentration. The data obtained are summarized in **Tables S10 – S12** and **Figures S27 – S32, ESI**. It seems from the PL data of the OEuCs:Host films that in all the single-EML devices, long-range Förster ET is the main process while direct carrier trapping is a sub-process except for **Device 3** of **Eu3** i.e., **Eu3** (4 wt%):26DCzPPy (10 nm) where carrier trapping is the main process and long-range Förster ET is a sub-process (PLQY = 32.2%; τ_{obs} = 467.9 μs). Among the fifteen single-EML

devices, **Device 2** of **Eu1**, **Device 3** of **Eu2** and **Device 3** of **Eu3** displayed the best EL performance with turn-on voltage ($V_{turn\text{-}on}$) = 2.9 V, B = 440 cd/m^2, η_c = 5.29 cd/A, η_p = 5.73 lm/W, EQE = 3.86%, $(CIE)_{x,y}$ = 0.61, 0.33 and FWHM = 7.95 nm for **Device 2** of **Eu1**, $V_{turn\text{-}on}$ = 2.9 V, B = 398 cd/m^2, η_c = 5.70 cd/A, η_p = 6.17 lm/W, EQE = 4.47%, $(CIE)_{x,y}$ = 0.64, 0.34 and FWHM = 8.00 nm for **Device 3** of **Eu2** and $V_{turn\text{-}on}$ = 3.1 V, B = 739 cd/m^2, η_c = 8.01 cd/A, η_p = 7.63 lm/W, EQE = 5.73%, $(CIE)_{x,y}$ = 0.62, 0.32 and FWHM = 8.23 nm for **Device 3** of **Eu3**, respectively. It is noteworthy that all the devices achieved a very low $V_{turn\text{-}on}$ (2.9 V – 3.1 V) which is substantially lower compared to reported OEuCs-based devices[8] and equates to the lowest reported value so far.[58] Such a low $V_{turn\text{-}on}$ could be attributed to barrier-free carrier injection, balanced carrier transport and recombination.[2, 55]

To further improve the EL performance of the present complexes, we fabricated fifteen double-EML devices (**Figure 6b**, five for each complex with the same OEuCs doping concentration) by inserting one more EML doped in an exciton/electron blocking material 4,4′,4″-tris-(carbazol-9-yl)-triphenylamine (TcTa) with a hole mobility value of 3.1 × 10^{-4} cm^2 V^{-1} s^{-1}.[59] Compared to the single-EML device, the double-EML device is expected to exhibit improved EL performance due to the wider recombination as noted by us and others.[55, 60] Moreover, the inclusion of TcTa could be propitious for reducing the biexcitonic quenching process in the OEuCs as noted by Liang et al.[60] and Kido et al.[27] Furthermore, the host TcTa in conjunction with another host (26DCzPPy) does not form any excited state exciplex as confirmed by Chen et al.[61] which generally decreases the EL efficiency.[56] The EL spectra of the devices displayed typical Eu(III) emission spectra identical to the single-EML devices with an obvious decrease in the host emission intensity implying either the improved long-range Förster ET or direct carrier trapping process. Moreover, the impact of this decrease in the host emission simultaneously resulted in purer red emission as evident from the improved $(CIE)_{x,y}$ colour coordinates, for example, for **Eu1**-based single-EML **Device 2** $(CIE)_{x,y}$ = 0.61, 0.33 while its double-EML counterpart i.e., **Device 7** = 0.65, 0.33.

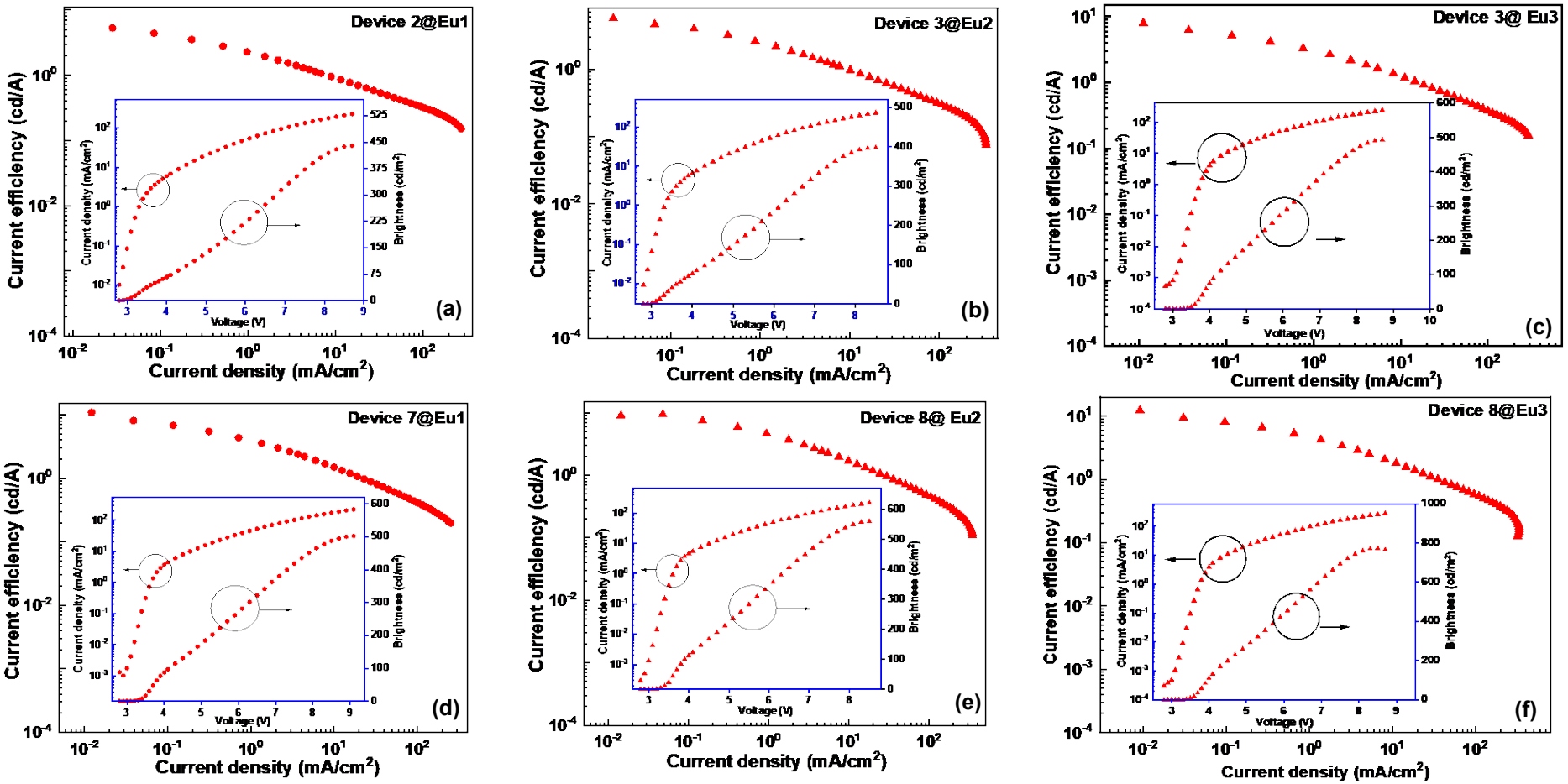

Figure 8: Current efficiency–current density characteristics of single-EML (a – c) and double-EML (d – f) devices of **Eu1**, **Eu2** and **Eu3**. Inset: *J-V-B* characteristics of devices.

Table 4: Key EL performances of **Eu1**, **Eu2** and **Eu3-**based OLEDs at J = 10 mA/cm^2.

Device	$V_{turn\text{-}on}$ (V)	B[a] (cd/m^2)	η_c (cd/A)	η_p(lm/W)	EQE_{max} (%)	$CIE_{x,y}$[a]	FWHM/nm[b]	EL Processes
Eu1								
6 [1]	3.1 [2.9]	542 [501]	9.53 [4.45]	9.66 [4.82]	7.38 [3.17]	(0.65, 0.33); [(0.57, 0.32)]	7.93 [8.05]	$(För)_{Main}$; $(CT)_{sub}$; [$(För)_{Main}$; $(CT)_{sub}$]
7 [2]	3.2 [2.9]	503 [440]	10.81 [5.29]	10.61 [5.73]	8.68 [3.86]	(0.65, 0.33); [(0.61, 0.33)]	8.00 [7.95]	$(För)_{Main}$; $(CT)_{sub}$; [$(För)_{Main}$; $(CT)_{sub}$]
8 [3]	3.2 [2.9]	546 [417]	10.47 [6.08]	10.28 [6.59]	7.98 [6.85]	(0.65, 0.33); [0.62, 0.33)]	7.99 [7.96]	$(För)_{Main}$; $(CT)_{sub}$; [$(För)_{Main}$; $(CT)_{sub}$]
9 [4]	3.2 [2.9]	544 [432]	8.98 [6.49]	8.81 [7.03]	6.68 [5.14]	(0.65, 0.33); [(0.63, 0.33)]	7.97 [7.97]	$(För)_{Main}$; $(CT)_{sub}$; [$(För)_{Main}$; $(CT)_{sub}$]
10 [1]	3.2 [2.9]	508 [443]	8.52 [4.24]	8.37 [4.59]	7.53 [3.82]	(0.64, 0.34); [(0.63, 0.34)]	7.93 [7.93]	$(För)_{Main}$; $(CT)_{sub}$; [$(För)_{Main}$; $(CT)_{sub}$]
Eu2								
6 [1]	3.1 [2.9]	586 [440]	5.27 [3.80]	4.87 [4.11]	3.08 [2.47]	(0.65, 0.34); [(0.62, 0.34)]	8.06 [7.99]	$(För)_{Main}$; $(CT)_{sub}$; [$(För)_{Main}$; $(CT)_{sub}$]
7 [2]	3.2 [2.9]	492 [380]	5.68 [4.43]	5.58 [5.12]	4.05 [3.37]	(0.65, 0.33); [(0.63, 0.34)]	8.08 [8.03]	$(För)_{Main}$; $(CT)_{sub}$; [$(För)_{Main}$; $(CT)_{sub}$]
8 [3]	3.2 [2.9]	561 [398]	9.42 [5.70]	8.97 [6.17]	5.85 [4.47]	(0.65, 0.33); [(0.64, 0.34)]	8.02 [8.00]	$(För)_{Main}$; $(CT)_{sub}$; [$(För)_{Main}$; $(CT)_{sub}$]
9 [4]	3.3 [3.0]	530 [402]	8.40 [4.15]	7.99 [4.34]	5.63 [3.23]	(0.65, 0.33); [(0.64, 0.34)]	8.02 [8.00]	$(För)_{Main}$; $(CT)_{sub}$; [$(För)_{Main}$; $(CT)_{sub}$]
10 [1]	3.3 [3.0]	496 316]	7.63 [4.02]	7.26 [4.20]	5.23 [2.73]	(0.65, 0.34); [(0.64, 0.34)]	8.04 [8.02]	$(För)_{Main}$; $(CT)_{sub}$; [$(För)_{Main}$; $(CT)_{sub}$]
Eu3								
6 [1]	3.3 [3.1]	784 [625]	10.62 [6.21]	10.11 [6.29]	7.98 [4.35]	(0.58, 0.31) [(0.55, 0.32)]	8.30 [8.34]	$(För)_{Main}$; $(CT)_{sub}$; [$(För)_{Main}$; $(CT)_{sub}$]
7 [2]	3.3 [3.1]	864 [671]	11.61 [7.96]	11.05 [8.06]	9.41 [5.92]	(0.62, 0.32) [(0.58, 0.32)]	8.25 [8.28]	$(För)_{Main}$; $(CT)_{sub}$; [$(För)_{Main}$; $(CT)_{sub}$]
8 [3]	3.3 [3.1]	773 [739]	12.32 [8.01]	11.73 [7.63]	10.2 [5.73]	(0.62, 0.32) [(0.62, 0.32)]	8.27 [8.23]	$(För)_{sub}$; $(CT)_{Main}$; [$(För)_{sub}$; $(CT)_{Main}$]
9 [4]	3.3 [3.1]	622 [524]	11.24 [6.32]	10.70 [6.41]	8.39 [5.25]	(0.62, 0.31) [(0.60, 0.32)]	8.33 [8.37]	$(För)_{Main}$; $(CT)_{sub}$; [$(För)_{Main}$; $(CT)_{sub}$]
10 [1]	3.4 [3.1]	681 [506]	8.06 [4.46]	7.24 [4.37]	4.96 [2.95]	(0.62, 0.33) [(0.61, 0.33)]	8.11 [8.13]	$(För)_{Main}$; $(CT)_{sub}$; [$(För)_{Main}$; $(CT)_{sub}$]

Values in the square parentheses are for single-EML devices; Förster = För, Carriers trapping (CT)

[a]$CIE_{x,y}$ at 10 mA/cm^2; [b]FWHM of electric-dipole $^5D_0 \rightarrow {}^7F_2$ transition

As expected, the best double-EML device of **Eu1** (**Device 6**; η_c = 10.81 cd/A; η_p = 10.61 lm/W; EQE = 8.68%), **Eu2** (**Device 8**; η_c = 9.42 cd/A; η_p = 8.97 lm/W; EQE = 5.85%) and **Eu3** (**Device 8**; η_c = 12.32 cd/A; η_p = 11.73 lm/W; EQE = 10.20%) exhibited almost 1.5-fold improvement in the electrophysical properties compared to their respective single-EML devices such as (**Device 2**)$_{Eu1}$, (**Device 3**)$_{Eu2}$ and (**Device 3**)$_{Eu3}$. To get the information regarding the dominant EL processes in the devices, the photophysical properties of the OEuCs: 26DCzPPy:OEuCs:TcTa films were determined. The data of the PLQY and excited state lifetime are summarized in **Tables S10 – S12** and **Figures S27 – S32, ESI, ESI**. Interestingly, **Device 6** of **Eu1** (PLQY = 59.4%) and **Device 8** of **Eu2**-based (PLQY = 59.2%) OEuCs: 26DCzPPy:OEuCs:TcTa films exhibited almost 20% – 24% reduction in their PLQY compared to the analogous single-EML films (**Device 2**; PLQY = 82.2% and **Device 3**; PLQY = 77.2%) and suggest the decrease in Förster ET efficiency. The results of the photophysical properties further suggest that the Förster ET started to become a sub-process and direct carrier trapping started to prevail. At this point of the discussion, it is thus safe and evident to say that high-performance OEuCs-based OLEDs could be envisioned where the direct carrier trapping process is the dominant EL process. This important point is confirmed by the **Eu3**-based double-EML (**Device 8**) device where the carrier trapping is the dominant EL process (PLQY = 44.3% of **Eu3**: 26DCzPPy:**Eu3**:TcTa film) resulting in the best overall performance such as B = 773 cd/m^2; η_c = 12.32 cd/A; η_p = 11.73 lm/W; EQE = 10.20%, $V_{turn\text{-}on}$ = 3.3 V. To the best of our knowledge, the overall performance of this device is the best among the family of OEuCs reported to date (**Chart 1**). Moreover, the improved EL performance of the **Eu3-**based device over other devices could also be due to the suppression of the biexcitonic quenching, a well-known effect regularly encountered in the OEuCs. This observation is further supported by the decrease in the EL intensity of the $^5D_1 \rightarrow {}^7F_2$ (520 – 550 nm) transition originating from another excited state $^5D_1$ (19,027 cm^{-1}) that lies very close to $^5D_0$ (17,293 cm^{-1}) excited state (**Figure 9** and **Figure S33, ESI**) and compares very well with the observation noted by Liang et al.[60] and Kido et al.[27] in the OEuC system. Thus, extending the recombination zone such as in the case of double-EML devices could be a beneficial strategy to curtail the deleterious biexcitonic quenching effect.

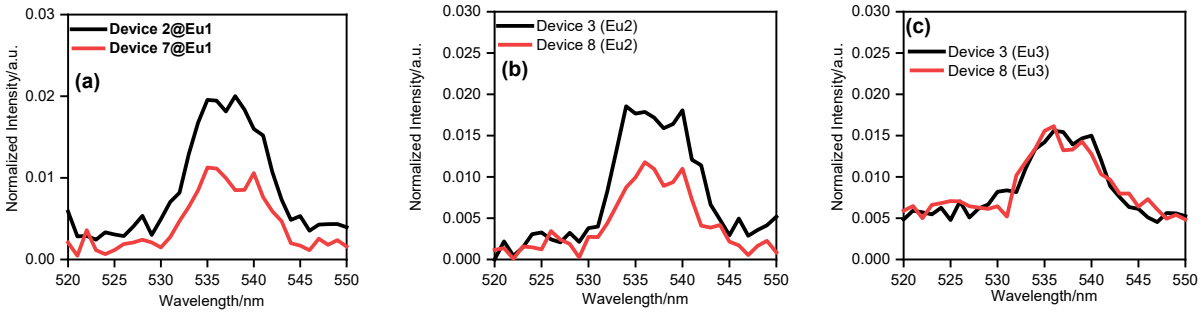

Figure 9: Magnified view of the region between 520 and 550 nm displaying the change intensity of the $^5D_1 \rightarrow {}^7F_2$ emission transition under electrical excitation operating at J = 10 mA/cm^2 for (a) **Eu1** (b) **Eu2** and (c) **Eu3**

Conclusion

In summary, three efficient red emitting nonacoordinated OEuCs have been designed, synthesized and successfully employed as the EML to fabricate R-OLEDs. The solid OEuCs under the UV excitation exhibited similar photophysical properties (**Table 1**) with Q_L^{Eu} values in the range of 59 – 62%, despite having different electron-rich substituent groups (furan, thiophene and naphthalene) at the 4' position of the ancillary TerPy ligand. This observation is further supported by the TD-DFT results which stemmed from the similar S_1 and T_1 MOs that formed these electronic states. Finally, the potential application of the complexes as EML to develop multilayer R-OLEDs have been demonstrated. Engineering of the device structure led to impressive EL performances with the electrophysical properties of **Device 6**; η_c = 10.81 cd/A; η_p = 10.61 lm/W; EQE_{max} = 8.68% for **Eu1**-based double EML device and **Device 8**; η_c = 12.32 cd/A; η_p = 11.73 lm/W; EQE_{max} = 10.20%, for **Eu3**-based double EML, respectively, dethroning the [Eu(dbm)$_3$BPhen]-based R-OLED with EQE_{max} = 7.5%. Furthermore, a careful investigation of the photophysical properties of the OEuC:Host film revealed that one might achieve high-performance OEuCs-based R-OLEDs where the long-range Förster ET starts to become a sub-process and direct carrier trapping starts to prevail, i.e., a dominant EL process together with extended recombination zone such as the case of double-EML device to curtail the undesirable biexcitonic quenching effect.

Associated Content: Supporting Information

The data that support the findings of this study are available in the supplementary material of this article**.**

Details of Theoretical Approaches; Determination of Ground State Geometry, Determination of Singlet (S) and Triplet State (T) Energy Levels, Modelling of Energy transfer (ET) Mechanism of the Sensitized Luminescence and Radiative emission rate (A_R) and PLQY

Details of Device Configurations; **Eu1**-Based devices, **Eu2** Based devices and **Eu3** Based devices

Tables; Spherical coordinates, Lowest values of CShMs (Continuous Shape Measures), Energy transfer rates, Theoretical intensity parameters, Photophysical properties of the **Eu1**-**Eu3** doped host films

Figures: FT-IR, NMR spectra, MALDI-TOF spectra, electronic absorption spectra, CIE-1931 chromaticity diagram, decay curves, Normalized EL spectra, current efficiency-current density characteristics curves, comparative PL spectra **Eu1**-**Eu3**-based films, comparative normalized EL spectra and additional references

Acknowledgements

MSK acknowledges His Majesty's Trust Fund for Strategic Research (Grant No. SR/SQU/SCI/CHEM/21/01) and The Ministry of Higher Education, Research and Innovation (MoHERI), Oman (Grant: RC/RG-SCI/CHEM/23/01) for funding. RI thanks HM's Trust Fund

for a postdoctoral fellowship. JDLD appreciates the financial support from the Brazilian funding agencies CAPES, CNPq (421733/2018-7) and FACEPE (APQ-0675-1.06/14). GSS thanks FAPITEC-SE (FAPITEC/SE/FUNTEC Nº 06/2022) for a scientific initiation fellowship. LZ is grateful for the financial aid from the National Natural Science Foundation of China (62174160). WYW thanks the Hong Kong Research Grants Council (PolyU 15305320), Guangdong-Hong Kong-Macao Joint Laboratory of Optoelectronic and Magnetic Functional Materials (2019B121205002), the CAS-Croucher Funding Scheme for Joint Laboratories (ZH4A), Research Institute for Smart Energy (CDAQ) and the Endowed Professorship in Energy from Miss Clarea Au (847S) both from the Hong Kong Polytechnic University for the financial support. PRR is grateful to the Engineering and Physical Sciences Research Council (EPSRC) for funding (Grant EP/K004956/1).

Conflict of Interest

The authors declare no conflict of interest.

References

(1) Ilmi, R.; Khan, M. S.; Sun, W.; Zhou, L.; Wong, W.-Y.; Raithby, P. R. A single component white electroluminescent device fabricated from a metallo-organic terbium complex. *J. Mater. Chem. C* **2019**, *7* (44), 13966-13975, DOI: https://doi.org/10.1039/C9TC04653D.

(2) Ilmi, R.; Sun, W.; Dutra, J. D. L.; Al-Rasbi, N. K.; Zhou, L.; Qian, P.-C.; Wong, W.-Y.; Raithby, P. R.; Khan, M. S. Monochromatic red electroluminescence from a homodinuclear europium(iii) complex of a β-diketone tethered by 2,2′-bipyrimidine. *J. Mater. Chem. C* **2020**, *8* (29), 9816-9827, DOI: https://doi.org/10.1039/D0TC02181D.

(3) Ilmi, R.; Zhang, D.; Tensi, L.; Al-Sharji, H.; Al Rasbi, N. K.; Macchioni, A.; Zhou, L.; Wong, W.-Y.; Raithby, P. R.; Khan, M. S. Salts of Lanthanide(III) Hexafluoroacetylacetonates [Ln = Sm(III), Eu(III) and Tb(III)] with Dipyridylammonium cations: Synthesis, characterization, photophysical properties and OLED fabrication. *Dyes Pigm.* **2022**, 110300, DOI: https://doi.org/10.1016/j.dyepig.2022.110300.

(4) Kitagawa, Y.; Tsurui, M.; Hasegawa, Y. Bright red emission with high color purity from Eu(iii) complexes with π-conjugated polycyclic aromatic ligands and their sensing applications. *RSC Adv.* **2022**, *12* (2), 810-821, DOI: https://doi.org/10.1039/D1RA08233G.

(5) Ilmi, R.; Khan, M. S.; Li, Z.; Zhou, L.; Wong, W.-Y.; Marken, F.; Raithby, P. R. Utilization of Ternary Europium Complex for Organic Electroluminescent Devices and as a Sensitizer to Improve Electroluminescence of Red-Emitting Iridium Complex. *Inorg. Chem.* **2019**, *58* (13), 8316-8331, DOI: https://doi.org/10.1021/acs.inorgchem.9b00303.

(6) Guan, H.; Qi, M.; Shi, L.; Liu, W.; Yang, L.; Dou, W. Ratiometric Luminescent Thermometer Based on the Lanthanide Metal–Organic Frameworks by Thermal Curing.

ACS Appl. Mater. Interfaces **2023**, *15* (14), 18114-18124, DOI: https://doi.org/10.1021/acsami.3c01897.

(7) Rocha, J.; Brites, C. D. S.; Carlos, L. D. Lanthanide Organic Framework Luminescent Thermometers. *Chem. Eur. J.* **2016**, *22* (42), 14782-14795, DOI: https://doi.org/10.1002/chem.201600860.

(8) Wang, L.; Zhao, Z.; Wei, C.; Wei, H.; Liu, Z.; Bian, Z.; Huang, C. Review on the Electroluminescence Study of Lanthanide Complexes. *Adv. Opt. Mater.* **2019**, *0* (0), 1801256, DOI: https://doi.org/10.1002/adom.201801256.

(9) Bunzli, J. C. G. On the design of highly luminescent lanthanide complexes. *Coord. Chem. Rev.* **2015**, *293* (0), 19-47, DOI: https://doi.org/10.1016/j.ccr.2014.10.013.

(10) Chen, Z.; Zhang, H.; Wen, D.; Wu, W.; Zeng, Q.; Chen, S.; Wong, W.-Y. A simple and efficient approach toward deep-red to near-infrared-emitting iridium(iii) complexes for organic light-emitting diodes with external quantum efficiencies of over 10%. *Chem. Sci.* **2020**, *11* (9), 2342-2349, DOI: https://doi.org/10.1039/C9SC05492H.

(11) Lee, C.-H.; Tang, M.-C.; Cheung, W.-L.; Lai, S.-L.; Chan, M.-Y.; Yam, V. W.-W. Highly luminescent phosphine oxide-containing bipolar alkynylgold(iii) complexes for solution-processable organic light-emitting devices with small efficiency roll-offs. *Chem. Sci.* **2018**, *9* (29), 6228-6232, DOI: https://doi.org/10.1039/C8SC02265H.

(12) Pander, P.; Daniels, R.; Zaytsev, A. V.; Horn, A.; Sil, A.; Penfold, T. J.; Williams, J. A. G.; Kozhevnikov, V. N.; Dias, F. B. Exceptionally fast radiative decay of a dinuclear platinum complex through thermally activated delayed fluorescence. *Chem. Sci.* **2021**, *12* (17), 6172-6180, DOI: https://doi.org/10.1039/D1SC07180G.

(13) Shi, Y.-Z.; Wu, H.; Wang, K.; Yu, J.; Ou, X.-M.; Zhang, X.-H. Recent progress in thermally activated delayed fluorescence emitters for nondoped organic light-emitting diodes. *Chem. Sci.* **2022**, *13* (13), 3625-3651, DOI: https://doi.org/10.1039/D1SC07180G.

(14) Al-Sharji, H.; Ilmi, R.; Khan, M. S. Recent Progress in Phenoxazine-Based Thermally Activated Delayed Fluorescent Compounds and Their Full-Color Organic Light-Emitting Diodes. *Topics in Current Chemistry* **2024**, *382* (1), 5, DOI: https://doi.org/10.1007/s41061-024-00450-3.

(15) Khan, M. S.; Ilmi, R.; Sun, W.; Dutra, J. D. L.; Oliveira, W. F.; Zhou, L.; Wong, W.-Y.; Raithby, P. R. Bright and efficient red emitting electroluminescent devices fabricated from ternary europium complexes. *J. Mater. Chem. C* **2020**, *8* (16), 5600-5612, DOI: https://doi.org/10.1039/D0TC00749H.

(16) Ilmi, R.; Li, X.; Al Rasbi, N. K.; Zhou, L.; Wong, W.-Y.; Raithby, P. R.; Khan, M. S. Two new red-emitting ternary europium(iii) complexes with high photoluminescence quantum yields and exceptional performance in OLED devices. *Dalton Trans.* **2023**, *52* (36), 12885-12891, DOI: https://doi.org/10.1039/D3DT02147E.

(17) Bin Mohd Yusoff, A. R.; Huckaba, A. J.; Nazeeruddin, M. K. Phosphorescent Neutral Iridium (III) Complexes for Organic Light-Emitting Diodes. *Top. Curr. Chem.* **2017**, *375* (2), 39, DOI: https://doi.org/10.1007/s41061-017-0126-7.

(18) Li, T.-Y.; Wu, J.; Wu, Z.-G.; Zheng, Y.-X.; Zuo, J.-L.; Pan, Y. Rational design of phosphorescent iridium(III) complexes for emission color tunability and their applications in OLEDs. *Coord. Chem. Rev.* **2018**, *374*, 55-92, DOI: https://doi.org/10.1016/j.ccr.2018.06.014.

(19) Wei, C.; Sun, B.; Cai, Z.; Zhao, Z.; Tan, Y.; Yan, W.; Wei, H.; Liu, Z.; Bian, Z.; Huang, C. Quantum Yields over 80% Achieved in Luminescent Europium Complexes by Employing Diphenylphosphoryl Tridentate Ligands. *Inorg. Chem.* **2018**, *57* (13), 7512-7515, DOI: https://doi.org/10.1021/acs.inorgchem.8b01028.

(20) Cai, Z.; Wei, C.; Sun, B.; Wei, H.; Liu, Z.; Bian, Z.; Huang, C. Luminescent europium(iii) complexes based on tridentate isoquinoline ligands with extremely high quantum yield. *Inorg. Chem. Front.* **2021**, *8* (1), 41-47, DOI: https://doi.org/10.1039/D0QI00894J.

(21) Al-Busaidi, I. J.; Ilmi, R.; Dutra, J. D. L.; Oliveira, W. F.; Haque, A.; Al Rasbi, N. K.; Marken, F.; Raithby, P. R.; Khan, M. S. Utilization of a Pt(ii) di-yne chromophore incorporating a 2,2'-bipyridine-5,5'-diyl spacer as a chelate to synthesize a green and red emitting d-f-d heterotrinuclear complex. *Dalton Trans* **2021**, *50* (4), 1465-1477, DOI: https://doi.org/10.1039/D0DT04198J.

(22) Al-Busaidi, I. J.; Ilmi, R.; Zhang, D.; Dutra, J. D. L.; Oliveira, W. F.; Al Rasbi, N. K.; Zhou, L.; Wong, W.-Y.; Raithby, P. R.; Khan, M. S. Synthesis and photophysical properties of ternary β-diketonate europium(III) complexes incorporating bipyridine and its derivatives. *Dyes Pigm.* **2022**, *197*, 109879, DOI: https://doi.org/10.1016/j.dyepig.2021.109879.

(23) Binnemans, K. Rare-earth beta-diketonates. In *Handbook on the Physics and Chemistry of Rare Earths*, K.A. Gschneidner, J. C. B., Pecharsky, V. K. Eds.; Vol. Volume 35; Elsevier, 2005; pp 107-272.

(24) Hasan, N.; Ilmi, R.; Iftikhar, K. Synthesis, X-ray crystal structure and photophysics of butterfly shape orange and red emanating polynuclear complexes of tris(dibenzoylmethanato)Ln(III) (Ln = Sm/Eu) and exo-bidentate 4,4'-bipyridine. *Photochem Photobiol Sci* **2024**, DOI: https://doi.org/10.1007/s43630-023-00519-w.

(25) Kido, J.; Nagai, K.; Okamoto, Y.; Skotheim, T. Electroluminescence from Polysilane Film Doped with Europium Complex. *Chem Lett* **1991**, *20* (7), 1267-1270, DOI: https://doi.org/10.1246/cl.1991.1267.

(26) Kido, J.; Nagai, K.; Okamoto, Y. Organic electroluminescent devices using lanthanide complexes. *J. Alloys Compd.* **1993**, *192* (1), 30-33, DOI: https://doi.org/10.1016/0925-8388(93)90176-N.

(27) Canzler, T. W.; Kido, J. Exciton quenching in highly efficient europium-complex based organic light-emitting diodes. *Org. Electron.* **2006**, *7* (1), 29-37, DOI: 10.1016/j.orgel.2005.10.004.

(28) Raj, D. B. A.; Biju, S.; Reddy, M. L. P. One-, two-, and three-dimensional arrays of Eu(3+)-4,4,5,5,5-pentafluoro-1-(naphthalen-2-yl)pentane-1,3-dione complexes: Synthesis, crystal structure and photophysical properties. *Inorg. Chem.* **2008**, *47* (18), 8091-8100, DOI: 10.1021/ic8004757.

(29) Naka, S.; Okada, H.; Onnagawa, H.; Tsutsui, T. High electron mobility in bathophenanthroline. *Appl. Phys. Lett.* **2000**, *76* (2), 197-199, DOI: https://doi.org/10.1063/1.125701.

(30) Wang, L.; Zhao, Z.; Wei, C.; Wei, H.; Liu, Z.; Bian, Z.; Huang, C. Review on the Electroluminescence Study of Lanthanide Complexes. *Adv. Opt. Mater* **2019**, *7* (11), 1801256, DOI: https://doi.org/10.1002/adom.201801256.

(31) Ilmi, R.; Wang, J.; Dutra, J. D. L.; Zhou, L.; Wong, W.-Y.; Raithby, P. R.; Khan, M. S. Efficient Red Organic Light Emitting Diodes of Nona Coordinate Europium Tris(β-diketonato) Complexes Bearing 4'-Phenyl-2,2':6',2''-terpyridine. *Chem. Eur. J.* **2023**, *n/a* (n/a), e202300376, DOI: https://doi.org/10.1002/chem.202300376.

(32) Judd, B. R. Optical Absorption Intensities of Rare-Earth Ions. *Phys. Rev.* **1962**, *127* (3), 750-761, DOI: https://doi.org/10.1103/PhysRev.127.750.

(33) Ofelt, G. S. Intensities of Crystal Spectra of Rare‐Earth Ions. *J. Chem. Phys.* **1962**, *37* (3), 511-520, DOI: http://dx.doi.org/10.1063/1.1701366.

(34) Ferreira da Rosa, P. P.; Kitagawa, Y.; Hasegawa, Y. Luminescent lanthanide complex with seven-coordination geometry. *Coord. Chem. Rev.* **2020**, *406*, 213153, DOI: https://doi.org/10.1016/j.ccr.2019.213153.

(35) Dutra, J. D.; Bispo, T. D.; Freire, R. O. LUMPAC lanthanide luminescence software: Efficient and user friendly. *J. Comput. Chem.* **2014**, *35* (10), 772-775, DOI: https://doi.org/10.1002/jcc.23542.

(36) Ilmi, R.; Haque, A.; Al-Busaidi, I. J.; Al Rasbi, N. K.; Khan, M. S. Synthesis and photophysical properties of hetero trinuclear complexes of tris β-diketonate Europium with organoplatinum chromophore. *Dyes Pigm.* **2019**, *162*, 59-66, DOI: https://doi.org/10.1016/j.dyepig.2018.10.011.

(37) Maroń, A.; Szlapa, A.; Klemens, T.; Kula, S.; Machura, B.; Krompiec, S.; Małecki, J. G.; Świtlicka-Olszewska, A.; Erfurt, K.; Chrobok, A. Tuning the photophysical properties of 4′-substituted terpyridines – an experimental and theoretical study. *Organic & Biomolecular Chemistry* **2016**, *14* (15), 3793-3808, DOI: https://doi.org/10.1039/C6OB00038J.

(38) Szlapa-Kula, A.; Małecka, M.; Machura, B. Insight into structure-property relationships of aryl-substituted 2,2′:6′,2″-terpyridines. *Dyes Pigm.* **2020**, *180*, 108480, DOI: https://doi.org/10.1016/j.dyepig.2020.108480.

(39) Ilmi, R.; Yin, J.; Dutra, J. D. L.; Al Rasbi, N. K.; Oliveira, W. F.; Zhou, L.; Wong, W.-Y.; Raithby, P. R.; Khan, M. S. Single component white-OLEDs derived from tris(β-diketonato) europium(iii) complexes bearing the large bite angle N^N 2-(4-thiazolyl)benzimidazole ligand. *Dalton Trans.* **2022**, *51* (37), 14228-14242, DOI: 10.1039/D2DT01873J.

(40) Ilmi, R.; Kansız, S.; Dege, N.; Khan, M. S. Synthesis, structure, Hirshfeld surface analysis and photophysical studies of red emitting europium acetylacetonate complex incorporating a phenanthroline derivative. *J. Photochem. Photobiol., A* **2019**, *377*, 268-281, DOI: https://doi.org/10.1016/j.jphotochem.2019.03.036.

(41) Ilmi, R.; Iftikhar, K. Synthesis, visible light absorption and luminescence of bipyrimidine bridged dinuclear lanthanide complexes of 2,4-pentanedione. *Inorg. Chem. Commun.* **2010**, *13* (12), 1552-1557, DOI: https://doi.org/10.1016/j.inoche.2010.09.010.

(42) Pinsky, M.; Avnir, D. Continuous Symmetry Measures. 5. The Classical Polyhedra. *Inorg. Chem.* **1998**, *37* (21), 5575-5582, DOI: https://doi.org/10.1021/ic9804925.

(43) Casanova, D.; Llunell, M.; Alemany, P.; Alvarez, S. The Rich Stereochemistry of Eight-Vertex Polyhedra: A Continuous Shape Measures Study. *Chem. Eur. J.* **2005**, *11* (5), 1479-1494, DOI: https://doi.org/10.1002/chem.200400799.

(44) Jacquemin, D.; Perpète, E. A.; Ciofini, I.; Adamo, C. Assessment of Functionals for TD-DFT Calculations of Singlet−Triplet Transitions. *J. Chem. Theory Comput.* **2010**, *6* (5), 1532-1537, DOI: https://doi.org/10.1021/ct100005d.

(45) Martin, R. L. Natural transition orbitals. *J. Chem. Phys.* **2003**, *118* (11), 4775-4777, DOI: https://doi.org/10.1063/1.1558471.

(46) Weissman, S. I. Intramolecular Energy Transfer The Fluorescence of Complexes of Europium. *J. Chem. Phys.* **1942**, *10* (4), 214-217, DOI: https://doi.org/10.1063/1.1723709.

(47) Graydon, O. OLEDs are more than just displays. *Nat Photonics* **2023**, *17* (3), 216-217, DOI: https://doi.org/10.1038/s41566-023-01160-w.

(48) Abusail, N. A.; Riyami, N. A.; Ilmi, R.; Khan, M. S.; Al-Rasbi, N. K. An efficient pink luminescent Eu(iii) coordination polymer excited on a blue LED chip. *J. Mater. Chem. C* **2023**, DOI: 10.1039/D3TC00215B.

(49) Ilmi, R.; Hasan, N.; Liu, J.; Mara, D.; Van Deun, R.; Iftikhar, K. Effect of 2,4,6-tri(2-pyridyl)-1,3,5-triazine on visible and NIR luminescence of lanthanide tris(trifluoroacetylacetonates). *J. Photochem. Photobiol., A* **2017**, *347*, 116-129, DOI: https://doi.org/10.1016/j.jphotochem.2017.06.031.

(50) Carneiro Neto, A. N.; Teotonio, E. E. S.; de Sá, G. F.; Brito, H. F.; Legendziewicz, J.; Carlos, L. D.; Felinto, M. C. F. C.; Gawryszewska, P.; Moura, R. T.; Longo, R. L.; Faustino, W. M.; Malta, O. L., Chapter 310 - Modeling intramolecular energy transfer in lanthanide chelates: A critical review and recent advances. In *Handbook on the Physics and Chemistry of Rare Earths*, Bünzli, J.-C. G., Pecharsky, V. K. Eds.; Vol. 56; Elsevier, 2019; pp 55-162.
(51) Dutra, J. D. L.; Lima, N. B. D.; Freire, R. O.; Simas, A. M. Europium Luminescence: Electronic Densities and Superdelocalizabilities for a Unique Adjustment of Theoretical Intensity Parameters. *Sci. Rep.* **2015**, *5* (1), 13695, DOI: https://doi.org/10.1038/srep13695.
(52) Borges, A. S.; Dutra, J. D. L.; Santos, G. S.; Diniz, R.; Kai, J.; Araujo, M. H. Theoretical and experimental spectroscopic investigation of new Eu(III)-FOD complex containing 2-pyrrolidone ligand. *Journal of Molecular Modeling* **2021**, *27* (10), 293, DOI: 10.1007/s00894-021-04883-1.
(53) Kasprzycka, E.; Carneiro Neto, A. N.; Trush, V. A.; Jerzykiewicz, L.; Amirkhanov, V. M.; Malta, O. L.; Legendziewicz, J.; Gawryszewska, P. How minor structural changes generate major consequences in photophysical properties of RE coordination compounds; resonance effect, LMCT state. *J. Rare Earths* **2020**, *38* (5), 552-563, DOI: https://doi.org/10.1016/j.jre.2020.02.001.
(54) Carneiro Neto, A. N.; Moura, R. T.; Aguiar, E. C.; Santos, C. V.; de Medeiros, M. A. F. L. B. Theoretical study of geometric and spectroscopic properties of Eu(III) complexes with Ruhemann's Purple ligands. *J. Lumin.* **2018**, *201*, 451-459, DOI: https://doi.org/10.1016/j.jlumin.2018.05.014.
(55) Ilmi, R.; Zhang, D.; Dutra, J. D. L.; Dege, N.; Zhou, L.; Wong, W.-Y.; Raithby, P. R.; Khan, M. S. A tris β-diketonate europium(III) complex based OLED fabricated by thermal evaporation method displaying efficient bright red emission. *Org. Electron.* **2021**, *96*, 106216, DOI: https://doi.org/10.1016/j.orgel.2021.106216.
(56) Uchida, M.; Adachi, C.; Koyama, T.; Taniguchi, Y. Charge carrier trapping effect by luminescent dopant molecules in single-layer organic light emitting diodes. *J Appl Phys* **1999**, *86* (3), 1680-1687, DOI: https://doi.org/10.1063/1.370947.
(57) Blumstengel, S.; Meinardi, F.; Tubino, R.; Gurioli, M.; Jandke, M.; Strohriegl, P. Long-range energy transfer of singlet and triplet excitations in dye-doped tris(phenylquinoxaline). *J. Chem. Phys.* **2001**, *115* (7), 3249-3255, DOI: https://doi.org/10.1063/1.1388050.
(58) Zhao, B.; Zhang, H.; Miao, Y.; Wang, Z.; Gao, L.; Wang, H.; Hao, Y.; Xu, B.; Li, W. Low turn-on voltage and low roll-off rare earth europium complex-based organic light-emitting diodes with exciplex as the host. *J. Mater. Chem. C* **2017**, *5* (46), 12182-12188, DOI: https://doi.org/10.1039/C7TC03694A.

(59) Kang, J.-W.; Lee, S.-H.; Park, H.-D.; Jeong, W.-I.; Yoo, K.-M.; Park, Y.-S.; Kim, J.-J. Low roll-off of efficiency at high current density in phosphorescent organic light emitting diodes. *Appl. Phys. Lett.* **2007**, *90* (22), 223508, DOI: https://doi.org/10.1063/1.2745224.
(60) Liang, C. J.; Wong, T. C.; Hung, L. S.; Lee, S. T.; Hong, Z. R.; Li, W. L. Self-quenching of excited europium ions in $Eu(DBM)_3$bath-based organic electroluminescent devices. *J. Phys. D: Appl. Phys.* **2001**, *34* (12), L61-L64, DOI: 10.1088/0022-3727/34/12/102.
(61) Chen, D.; Wang, Z.; Wang, D.; Wu, Y.-C.; Lo, C.-C.; Lien, A.; Cao, Y.; Su, S.-J. Efficient exciplex organic light-emitting diodes with a bipolar acceptor. *Org. Electron.* **2015**, *25*, 79-84, DOI: https://doi.org/10.1016/j.orgel.2015.06.022.